Single-cell analysis of regions of interest (SCARI) using a photosensitive tag

Leun, A.M. van der; Hoekstra, M.E.; Reinalda, L.; Scheele, C.L.G.J.; Toebes, M.; Graaff, M.J. van de; ... ; Schumacher, T.N.

nature chemical biology

ARTICLES

https://doi.org/10.1038/s41589-021-00839-x

Check for updates

Single-cell analysis of regions of interest (SCARI) using a photosensitive tag

Anne M. van der Leun[1,12], Mirjam E. Hoekstra[1,12], Luuk Reinalda[2], Colinda L. G. J. Scheele[3,8], Mireille Toebes[1], Michel J. van de Graaff[2,9], Linda Y. Y. Chen[3], Hanjie Li[4,10], Akhiad Bercovich[5], Yaniv Lubling[5,11], Eyal David[4], Daniela S. Thommen[6], Amos Tanay[5], Jacco van Rheenen[3], Ido Amit[4], Sander I. van Kasteren[2,13] ✉ and Ton N. Schumacher[1,7,13] ✉

The functional activity and differentiation potential of cells are determined by their interactions with surrounding cells. Approaches that allow unbiased characterization of cell states while at the same time providing spatial information are of major value to assess this environmental influence. However, most current techniques are hampered by a tradeoff between spatial resolution and cell profiling depth. Here, we develop a photocage-based technology that allows isolation and in-depth analysis of live cells from regions of interest in complex ex vivo systems, including primary human tissues. The use of a highly sensitive 4-nitrophenyl(benzofuran) cage coupled to a set of nanobodies allows high-resolution photo-uncaging of different cell types in areas of interest. Single-cell RNA-sequencing of spatially defined CD8$^+$ T cells is used to exemplify the feasibility of identifying location-dependent cell states. The technology described here provides a valuable tool for the analysis of spatially defined cells in diverse biological systems, including clinical samples.

Methods for the in-depth characterization of individual cells, such as single-cell transcriptomics and proteomics, form an essential approach for our understanding of cellular function in human tissues. Although these technologies are well suited to describe the diversity of physiological and pathophysiological cell states, information on the spatial localization of the analyzed cells is lost upon tissue dissociation. However, knowledge about the spatial context of individual cells is critical to understanding how locoregional differences in environmental signals (for example, through cell–cell interactions or soluble mediators) impact cellular state and cell differentiation. For example, within human cancers, immune cells are found both at peritumoral and intratumoral sites, and intratumoral immune cells may be further subdivided, for instance into cells located within tumor cell nests and tertiary lymphoid organs. However, the relationship between cell state and any of these different cell locations is poorly understood[1]. Classical methods that are used to simultaneously assess the localization and phenotypic properties of individual cells, such as immunohistochemistry and confocal microscopy, are limited by the number of parameters that can be analyzed. Although next-generation imaging techniques, such as imaging mass cytometry[2], multi ion beam imaging by time of flight (MIBI-TOF)[3] and co-detection by indexing (CODEX)[4], allow the analysis of multiple markers on tissue slides, these technologies still require upfront decisions on the genes or proteins that are assessed or lack the resolution offered by the former techniques.

The combination of the spatial resolution from microscopy approaches with the unbiased profiling capacity of single-cell techniques has the potential to allow the ab initio analysis of the relationship between cell state and cellular localization. Work in transgenic mouse models has demonstrated that the localized switching of photoactivatable proteins, such as photoactivatable green fluorescent protein, Dronpa or Dendra, allows the analysis of single-cell transcriptomes in regions of interest with high spatial resolution[5]. However, approaches based on the genetic encoding of photosensitive proteins are not applicable to primary human tissues. To address this need, a number of methods, including Slide-seq[6] and related spatial transcriptomics approaches[7–12], have been developed that can be used to couple transcriptome data and spatial information from cells in human tissues. In slide-based spatial transcriptomics approaches, messenger RNA (mRNA) molecules from tissue slices are transferred to barcode-labeled surfaces[6–8], thereby providing the possibility to perform an unbiased analysis of transcriptional activity at defined sites, but with the caveat that the gene expression patterns obtained are often averages from multiple cells. On the other hand, the specific labeling of spatially defined cells in live tissues followed by single-cell analysis of those cells upon dissociation does not suffer from this limitation. Recent work has demonstrated how local uncaging of DNA barcodes that are protected by photolabile 6-nitropiperonyloxylmethyl (NPOM) groups can be used to specifically mark cells in areas of interest in tissue sections[13]. In this article, we develop a distinct technology with a unique set of features that exploits a 4-nitrophenyl(benzofuran) (NPBF) caged protein tag to

[1]Division of Molecular Oncology & Immunology, Oncode Institute, The Netherlands Cancer Institute, Amsterdam, Netherlands. [2]Department of Bio-Organic Synthesis, Leiden Institute of Chemistry, Leiden University, Leiden, Netherlands. [3]Division of Molecular Pathology, Oncode Institute, The Netherlands Cancer Institute, Amsterdam, Netherlands. [4]Department of Immunology, Weizmann Institute of Science, Rehovot, Israel. [5]Department of Computer Science and Applied Mathematics and Department of Biological Regulation, Weizmann Institute, Rehovot, Israel. [6]Division of Molecular Oncology & Immunology, The Netherlands Cancer Institute, Amsterdam, Netherlands. [7]Department of Hematology, Leiden University Medical Center, Leiden, Netherlands. [8]Present address: VIB-KULeuven Center for Cancer Biology, Leuven, Belgium. [9]Present address: SeraNovo, Leiden, Netherlands. [10]Present address: Shenzhen Institute of Synthetic Biology, Shenzhen, China. [11]Present address: Cancer Research UK Cambridge Institute, Cambridge, UK. [12]These authors contributed equally: Anne M. van der Leun, Mirjam E. Hoekstra. [13]These authors jointly supervised this work: Sander I. van Kasteren, Ton N. Schumacher. ✉e-mail: s.i.van.kasteren@chem.leidenuniv.nl; t.schumacher@nki.nl

uniformly label cells in situ in live, intact human tissue. The use of the NPBF group allows highly efficient uncaging under mild conditions (that is, using low-intensity violet light), resulting in minimal phototoxicity. In addition, the implementation of a signal switch system, in which uncaging leads to the simultaneous loss of a first signal and gain of a second signal, allows superior separation of uncaged and caged cells. The 'single-cell analysis of regions of interest' (SCARI) technology that we describe can be used to specifically isolate cell populations from defined regions with high spatial resolution, and we exemplify the value of this approach through single-cell mRNA sequencing of human T cells at defined sites.

Results

Conceptual approach to achieve localized cell marking. To label cells at specific tissue sites with minimal phototoxicity, we set out to create a photosensitive molecule in which a detectable group was shielded by a photolabile protecting group (PPG). The most commonly used PPGs for photo-uncaging in biological systems are the *o*-nitrobenzyl-based chromophores (for example, 6-nitroveratryloxycarbonyl (NVOC) and NPOM), which have, amongst others, been used to study T-cell activation kinetics[14], the liberation of pro-drugs[15–18] and variation in immune cell states[13]. These chromophores, however, have a low quantum yield ($\varphi_u^{NVOC} = 0.0013$, $\varphi_u^{NPOM} = 0.0075$) and therefore require either long light exposure or high-intensity light to remove the photolabile group, potentially resulting in light-induced cellular damage[19]. In addition, in the case of NVOC, photo-uncaging is accompanied by the release of toxic benzaldehyde by-products[20,21]. The recently reported NPBF chromophore has a superior uncaging efficiency ($\varphi_u^{NPBF} = 0.09$)[22] and, although less information is available regarding the toxicity of the released by-products upon light exposure, this makes it an attractive starting point for the design of a photo-uncaging system. To achieve an optimal distinction between uncaged and caged cells, we designed an approach in which removal of the NPBF chromophore simultaneously leads to the loss of a first detectable (fluorescent) signal and gain of a second signal. To accomplish this, we developed a photosensitive tag (PsT) containing a FLAG-peptide (DYKDDDDK) that is protected by an Alexa Fluor 594 (AF594)-conjugated NPBF-protecting group (Fig. 1, first panel). We envisioned that this photocage would interfere with the binding of αFLAG antibodies, and uncaging of the FLAG-tag could thus be used to simultaneously release the AF594 dye and create a novel antibody binding site. To this end, a bifunctional NPBF photocleavable linker bearing an *N*-hydroxysuccinimide (NHS) carbonate on one end and an alkyne handle on the other was developed to allow orthogonal installation of the photocage on the FLAG-epitope and clicking of the alkyne handle of the photocage with an azide-functionalized fluorophore[23]. To be able to label specific cell types, the caged FLAG-tag was subsequently coupled to cell lineage-specific nanobodies through sortase-based reactions[24]. For this purpose, the canonical FLAG-octapeptide sequence (DYKDDDDK) was extended by three N-terminal glycines[25] to allow conjugation to LPXTG-modified nanobodies. In addition, a cysteine was placed between the N-terminal GGG and FLAG-tag sequence to prevent aspartimide formation[26], resulting in the final sequence GGGCDYKDDDDK. Depending on whether labeling of nanobodies is performed under reducing or oxidizing conditions, the presence of the cysteine residue yields either a single copy or two copies of the (caged) FLAG-epitope per nanobody (see the following for further characterization). The FLAG-epitope contains two lysine residues that are suitable for installing the photocage. Previous work has demonstrated that the C-terminal lysine does not substantially influence antibody binding, and is thus not suitable for the intended epitope deprotection strategy[27]. By contrast, it has been demonstrated that the N-terminal DYKD sequence of the FLAG-peptide can be used in immunological detection procedures[28], making it plausible that modification of the side-chain amine of this lysine residue (Lys7) would abolish antigen recognition for at least some αFLAG antibodies.

Synthesis of the photosensitive tag. The bifunctional NPBF photocage **1** was synthesized essentially as reported previously (Extended Data Figs. 1a, **2**–**12**, final product **1**)[23]. The modified FLAG-tag sequence GGGCDYKDDDDK was synthesized using acid-labile 4-methoxytrityl (Mmt) as the protecting group for the amine on Lys7, to allow orthogonal deprotection of this side chain. An optimized method for Fmoc-based microwave-assisted solid-phase peptide synthesis (SPPS), which prevents racemization and aspartimide formation, was applied to obtain the core oligopeptide **13** (Extended Data Fig. 1b)[29]. Mmt was removed under mild conditions (1% trifluoroacetic acid, TFA), and the side-chain amine of the Lys7 of **14** was reacted with the NHS carbonate of **1** to yield photocaged peptide **15** on-resin. After cleavage from the resin and deprotection of all other amino acids, the photocaged peptide **16** was purified by reverse-phase HPLC, followed by copper-catalyzed alkyne-azide cycloaddition with AF594 azide, yielding the PsT (Fig. 1, first panel and Extended Data Fig. 1b). Analysis of the uncaging efficiency of the PsT using 420-nm light demonstrated a $t_{1/2}$ of less than 5 min (Extended Data Fig. 1c).

Characterization of photosensitive αCD8 antibody reagents. To determine the feasibility of using PsT-labeled antibodies to selectively mark cells at defined tissue sites (Fig. 1), we generated fluorochrome-labeled camelid heavy-chain-only fragments (nanobodies) specific for the human T-cell marker CD8. Nanobodies display superior tissue penetration capacity compared to regular antibodies due to their small size (~15 kDa versus ~150 kDa)[30], a property that may be particularly useful for in vivo or ex vivo staining of intact tissues with dense cellular and extracellular structures. To probe the effect of avidity on the selectivity and stability of cell marking, we first designed monomeric and dimeric fluorochrome-labeled αCD8 nanobodies ($\alpha CD8^{M}$ or $\alpha CD8^{D}$, respectively). Subsequently, the stability of cell labeling when using either monomeric or dimeric αCD8 nanobodies was determined by staining two separate human $CD8^+$ T-cell populations with αCD8 nanobodies coupled to distinct fluorochromes and subsequent mixing. Following mixing of the differentially labeled cell populations, a rapid exchange of monomeric αCD8 nanobodies was observed. By contrast, for two different tested dimeric αCD8 nanobody clones ($\alpha CD8^{D-1}$ and $\alpha CD8^{D-2}$), highly stable cell binding was observed (Extended Data Fig. 2a,b), a property essential for the intended localized cell marking.

We subsequently generated $\alpha CD8^{D-1}$ nanobodies labeled with the PsT (Extended Data Fig. 3a) and determined whether the NPBF cage prevents antibody binding to the FLAG-tag. For this purpose, primary human $CD8^+$ T cells were stained with FLAG-tag $\alpha CD8^{D-1}$ nanobodies that either contained or lacked the NPBF cage ($\alpha CD8^{D-1}$-PsT and $\alpha CD8^{D-1}$-T, respectively), and accessibility of the FLAG-epitope was probed using a set of different αFLAG antibodies. Notably, although certain αFLAG antibodies were insensitive to the NPBF cage (Extended Data Fig. 3b), binding of the D6W5B antibody was reduced to background levels upon caging of the lysine side chain (Extended Data Fig. 3c).

To understand whether photo-uncaging could be used to both remove the cage, and thereby the AF594 signal, and gain an αFLAG signal under conditions with limited toxicity, PsT-labeled cells were photo-uncaged by exposure to 405-nm laser light, and then stained with αFLAG antibody. Flow cytometric analyses of the resulting cell populations demonstrated that uncaging both led to the intended loss in AF594 signal and gain in αFLAG antibody binding (Fig. 2a,b and Extended Data Fig. 4). Comparison of the uncaging efficiency of nanobodies that contained one or

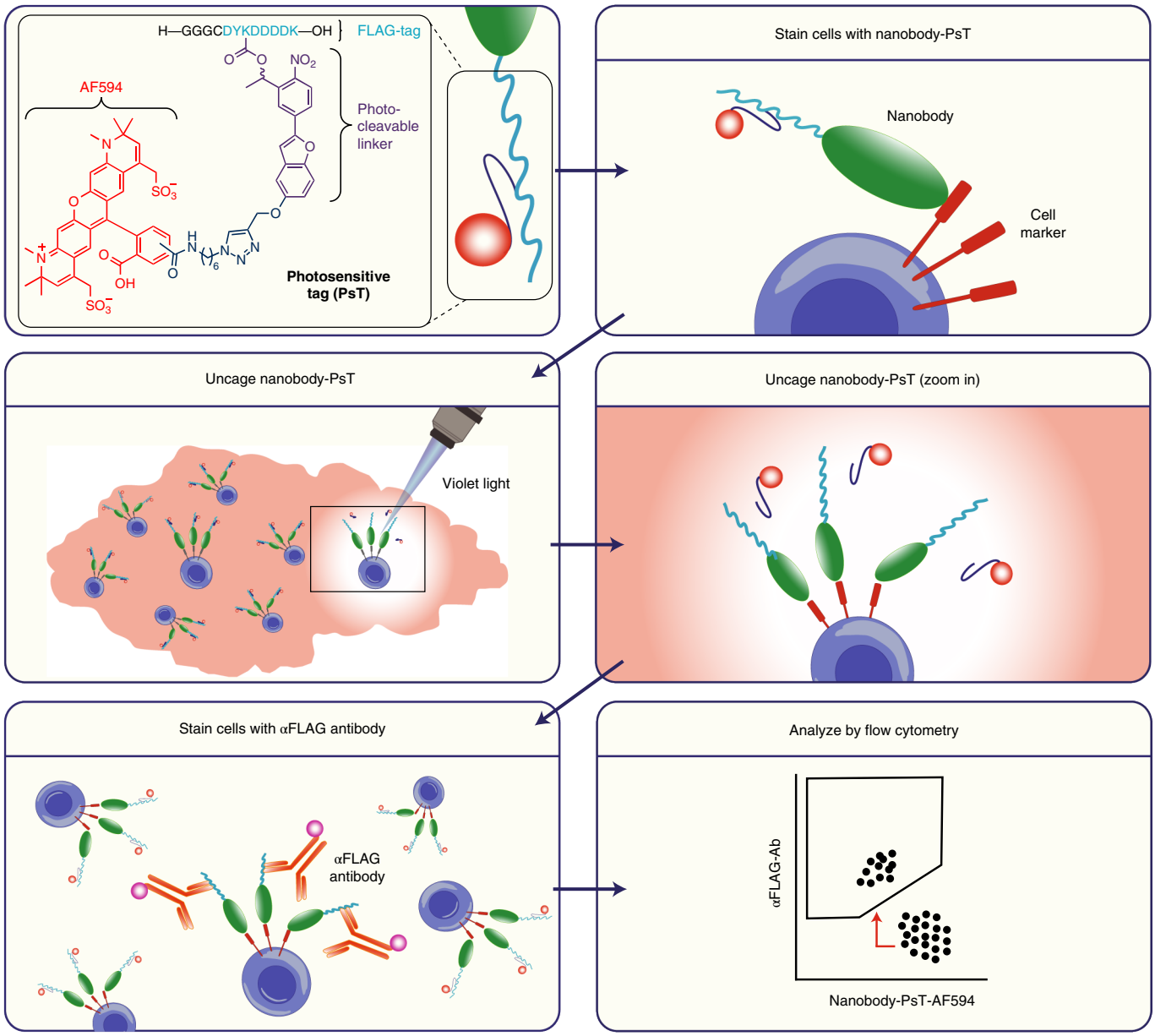

Fig. 1 | Schematic approach for single-cell analysis of regions of interest. Schematic representation of the experimental approach for spatial analysis of cells. Nanobodies are labeled with the PsT, which consists of a FLAG-tag caged by an NPBF photosensitive group coupled to an AF594 fluorochrome. Synthesis of the PsT is shown in Extended Data Fig. 1b. Cells or tissues are stained with PsT-labeled nanobody, and PsT-stained cells in areas of interest are uncaged using 405-nm violet light. After cell collection or tissue dissociation, single-cell suspensions are stained with an αFLAG antibody that only binds to the uncaged FLAG-tag. Cells from the area of interest can thus, after uncaging, be identified on the basis of both their low AF594 signal and high αFLAG signal. Isolation of cells based on both properties (that is, AF594^{low} αFLAG^{high} cells as cells within the area of interest and AF594^{high} αFLAG^{low} cells as cells outside the area of interest) results in an optimal separation between the uncaged and caged cell populations.

two copies of the PsT (Extended Data Fig. 5a) showed equally efficient separation between uncaged (AF594^{low} αFLAG^{high}) and caged (AF594^{high} αFLAG^{low}) cells for both molecules (Extended Data Fig. 5b). Notably, although uncaging was already maximally effective at 865 µW mm^{-2} of violet light exposure, cell viability remained unaffected (>95%) up to 1,440 µW mm^{-2} (Fig. 2c and Extended Data Fig. 6a,b). To explore the specificity of uncaging, we uncaged increasing surface areas of microwells containing CD8$^+$ T cells in a heterogeneous population of peripheral blood mononuclear cells (PBMCs). Importantly, the fraction of uncaged surface area was tightly correlated with the fraction of uncaged CD8$^+$ T cells, as measured by flow cytometry (Extended Data Fig. 6c). Of note, mixing of cell samples that did or did not contain an uncaged CD8$^+$ T-cell population showed no detectable αCD8^{D-1}-PsT exchange between cells, confirming the stable binding of αCD8^{D-1}-PsT throughout the sample processing pipeline (Extended Data Fig. 6d). To explore the resolution of our method, we uncaged areas with decreasing dimensions (Fig. 2d). CD8$^+$ T cells from areas as small as 3×10^3 µm^2 (58 × 58 µm), corresponding to 30–60 cells, could be clearly and reproducibly distinguished from background (Fig. 2e,f). Finally, the flexibility of the method was demonstrated by the successful uncaging of cell populations labeled with two additional PsT-linked nanobodies, specific for either the CD47 immune checkpoint expressed by

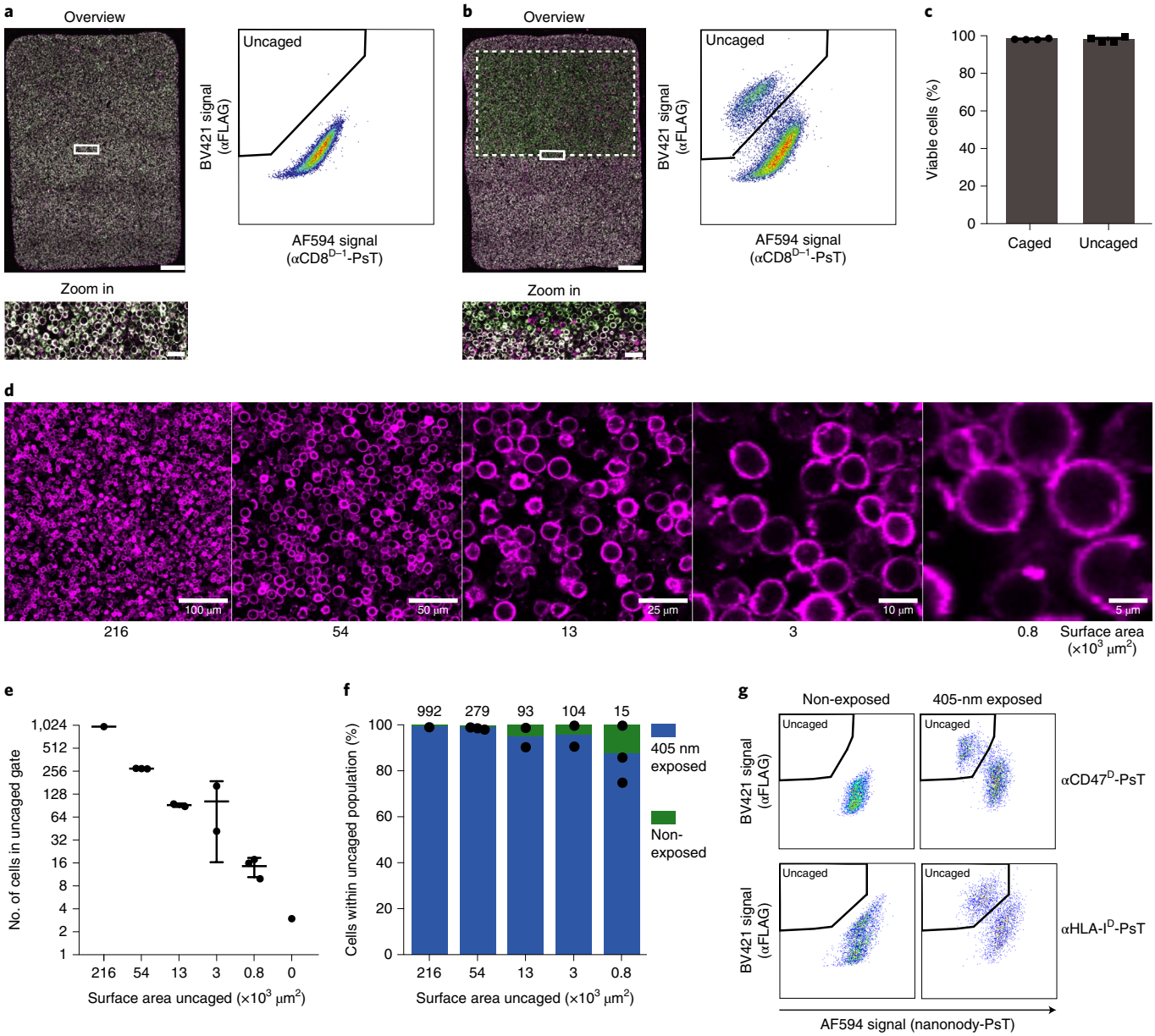

Fig. 2 | Uncaging of PsT-labeled primary human CD8⁺ T cells. a, Left: confocal image of CD8⁺ T cells stained with αCD8^{D-1}-PsT and αCD8^{D-2}-FITC, shown in magenta and green, respectively. Overlapping signals are shown in white. The area outlined by a solid line is shown at higher magnification at the bottom. Scale bars, 100 μm (top) and 10 μm (bottom). Right: flow cytometry analysis of αCD8^{D-1}-PsT-labeled CD8⁺ T cells after αFLAG staining. Representative data from three independent experiments are shown. **b**, Left: confocal image of CD8⁺ T cells as in **a**. The dashed box indicates the area of uncaging by 405-nm light exposure. The area outlined by a solid line is shown at higher magnification at the bottom. Scale bars, 100 μm (top) and 10 μm (bottom). Right: flow cytometry analysis of CD8⁺ T cells following uncaging and subsequent staining with αFLAG antibody. Representative data from three independent experiments are shown. **c**, Viability of uncaged and caged CD8⁺ T cells from partially uncaged samples (as in **b**), as measured by flow-cytometric analysis of IR-dye live–dead staining. Data from three independent experiments are shown ($n = 2$ technical replicates for one experiment), and the plot shows mean + s.d. **d**, Representative microscopy images of uncaged areas with decreasing dimensions (ranging from 216×10^3 μm² (465 × 465 μm) to 0.8×10^3 μm² (29 × 29 μm)) containing CD8⁺ T cells stained with αCD8^{D-1}-PsT, shown in magenta. Data are representative of three independent experiments. **e**, Cell recovery upon uncaging of areas of the indicated size. Single data points represent the number of uncaged αCD8^{D-1}-PsT cells recovered in flow-cytometry analysis ($n = 1$–3 technical replicates per condition). Data are representative of three independent experiments, and the plot shows mean ± s.d. **f**, Quantification of true uncaging events over background by flow cytometry, after mixing cells from exposed and non-exposed samples. Bars represent the fraction of cells derived from exposed (truly uncaged, blue) or non-exposed samples (background, green) within the uncaged (AF594^{low} αFLAG^{high}) population. Total cell numbers (mean across replicates) within the uncaged gate are depicted on top ($n = 1$–3 technical replicates). Data are representative of three independent experiments. **g**, Flow-cytometry analysis showing uncaging of BA/F3 cells and human T cells stained with CD47 (αCD47^{D}-PsT) or HLA class I (αHLA-I^{D}-PsT) nanobodies, respectively. Data are obtained from a single experiment ($n = 2$ technical replicates).

myeloid cells, or the HLA class I molecules that are expressed by all nucleated cells (Fig. 2g).

Local uncaging in human tumor tissue and cell systems. To determine the feasibility of local uncaging in more complex biological structures, we tested the efficiency of staining and uncaging of CD8$^+$ T cells in viable human melanoma and non-squamous cell lung cancer (NSCLC) tissue. CD8$^+$ T cells present within viable human tumor material were readily detected upon staining with αCD8^{D-1}-PsT and αCD8^{D-2}-FITC (Fig. 3a). Furthermore, uncaging of the αCD8^{D-1}-PsT in areas of melanoma and NSCLC tumors resulted in a discrete population of AF594^{low} and αFLAG^{high} cells that were not observed in non-exposed tumor tissue (Fig. 3b), while the viability of these CD8$^+$ T cells remained unaffected (Fig. 3c).

To understand whether local uncaging could be used to identify location-dependent differences in cell states, we developed an in vitro cell system in which specific differences in cell states could be induced in a controlled setting (Fig. 3d). With this aim, adjacent islands of tumor cells that either lacked or expressed the HLA class I-restricted CDK4$_{R>L}$ neoantigen (Katushka-positive Ag$^-$ regions and GFP-positive Ag$^+$ regions, respectively) were generated. αCD8^{D-1}-PsT-labeled CD8$^+$ T cells specific for the CDK4$_{R>L}$ neoantigen were added to the cultures, with the expectation that T-cell activation would be induced in Ag$^+$ areas, but not in Ag$^-$ areas. Following 4 h of co-culture, CD8$^+$ T cells in either Ag$^+$ or Ag$^-$ areas were uncaged and then isolated by cell sorting (Fig. 3e). As a control, uncaged CD8$^+$ T cells were isolated from separate control cultures that only contained Ag$^+$ tumor cells or Ag$^-$ tumor cells. To test for spatial differences in T-cell activation, expression of the T-cell activation marker CD69 was compared for uncaged T cells that were derived from Ag$^+$ tumor-cell areas or Ag$^-$ tumor-cell areas. Consistent with expectations, AF594^{low} αFLAG^{high} CD8$^+$ T cells isolated from cultures in which uncaging was limited to Ag$^+$ tumor-cell areas displayed a substantial increase in CD69 expression relative to AF594^{low} αFLAG^{high} CD8$^+$ T cells from cultures in which uncaging was limited to Ag$^-$ tumor-cell areas (Fig. 3f,g).

Single-cell analysis of spatially defined CD8$^+$ T cells. We subsequently analyzed the transcriptomes of CD8$^+$ T cells isolated from Ag$^+$ and Ag$^-$ regions by massive parallel single-cell mRNA sequencing (MARS-seq)[31]. To determine whether local uncaging could be used to reveal location-dependent transcriptional differences, two parallel approaches were used. First, in a cell-centric approach, cell states were identified using cells from all conditions, and enrichment of specific transcriptional states in uncaged (AF594^{low} αFLAG^{high}) cells from either Ag$^+$ or Ag$^-$ areas was determined. Second, in a gene-set-centric approach, gene modules were defined based on the most variable genes in the full dataset, and differential expression of such gene modules between uncaged cells from Ag$^+$ and Ag$^-$ areas was analyzed.

To test for location-dependent differences in cell states, T cells from all conditions were partitioned into groups of cells ('meta-cells') with similar gene expression patterns, using the MetaCell algorithm (Supplementary Data 1)[32]. This partitioning revealed a large group of T cells that unanimously expressed T-cell activation markers such as *GZMB* and *CRTAM* (T-act), as well as a second large group of T cells that lacked expression of these marker genes (T-non-act, Fig. 4a and Extended Data Fig. 7a,b; further characterization is shown in the following). Notably, comparison of the cell states of uncaged and caged cells under control conditions (that is, that only contained Ag$^+$ tumor cells or only contained Ag$^-$ tumor cells) demonstrated that the uncaging procedure did not influence the cell states (Extended Data Fig. 7c). Furthermore, uncaging did not induce detectable expression of stress-related genes (Fig. 4b), demonstrating that the PsT uncaging method allows for in-depth analysis of viable cells with unperturbed cell-intrinsic gene expression patterns.

Subsequent comparison of the cell states of uncaged CD8$^+$ T cells derived from Ag$^+$ or Ag$^-$ areas (Extended Data Fig. 7d) revealed that the T-act state was highly enriched in Ag$^+$ areas (77%), while T-non-act cells showed an increased abundance in Ag$^-$ areas (82%, Fig. 4c and Extended Data Fig. 7e). Similarly, at the subgroup level (T-act^1, T-act^2 and T-non-act$^{1-3}$, Extended Data Fig. 7b), a substantial enrichment of activated CD8$^+$ T-cell states was observed in Ag$^+$ areas, while all three non-activated CD8$^+$ T-cell populations showed enrichment in the Ag$^-$ region (Fig. 4c). To determine whether the uncaged cell population was homogeneous or whether cell pools with a lower level of uncaging (that is, cells with intermediate AF594 and αFLAG signal) showed an increased contamination with adjacent cells (for example, with partially uncaged cells showing a non-activated cell state in samples in which uncaging was aimed at Ag$^+$ areas), we divided the uncaged T cells from Ag$^+$ areas into bins based on their level of uncaging (bin 1 containing 'highly uncaged' cells to bin 5 containing 'lowly uncaged' cells). Notably, enrichment in activated T-cell states was consistently observed across bins (Fig. 4d), demonstrating the efficient separation of cells located in different areas.

To assess whether variability in the data at the gene level could be mapped to the location of cells (that is, in Ag$^+$ or Ag$^-$ areas), we next selected the top 30 genes with the highest variance throughout the entire dataset (Fig. 5a,b and Supplementary Data 2). This list contained a considerable number of genes encoding soluble mediators, such as Interferon Gamma *(IFNG)*, C-C Motif Chemokine Ligand 4 (*CCL4*) and C-X-C Motif Chemokine Ligand 8 (*CXCL8*), factors that are known for their role in inflammation[33–35]. Furthermore, a substantial portion (67%) of the top 30 most variable genes showed

Fig. 3 | Uncaging of CD8$^+$ T cells in primary human tumor tissue and cell culture systems. a, Confocal images of CD8$^+$ T cells stained with αCD8^{D-1}-PsT and αCD8^{D-2}-FITC in viable human melanoma and NSCLC tumor tissue. CD8$^+$ T cells are depicted in green and collagen in white. Enlarged areas are indicated by the numbered white boxes in the main panel. Scale bars, 100 μm (overview) and 10 μm (enlarged images). Images are representative of one (NSCLC) and three (melanoma) experiments. **b**, Uncaging of αCD8^{D-1}-PsT-labeled CD8$^+$ T cells in human tumor tissue. The indicated samples were left unexposed (top) or locally exposed to 405-nm light (bottom). **c**, Viability of CD8$^+$ T cells from human tumor tissue. The viability of CD8$^+$ T cells, measured by flow-cytometric analysis of IR-dye stain, from locally uncaged regions (AF594^{low} αFLAG^{high}), is compared to the viability of CD8$^+$ T cells from non-exposed areas (AF594^{high}αFLAG^{low}) ($n = 4$ technical replicates per group). Representative data from two experiments are presented as mean + s.d. **d**, Approach to validate the ability to identify local differences in cell state. **e**, Confocal images of co-cultures of Ag-specific CD8$^+$ T cells with tumor-cell islands. Top: island cultures containing Ag$^+$ tumor-cell areas (green) surrounded by Ag$^-$ tumor-cell areas (magenta). Bottom: control cultures that only contain Ag$^+$ tumor cells (bottom, left) or Ag$^-$ tumor cells (bottom, right). White dashed boxes indicate regions uncaged by 405-nm light exposure. Scale bars, 1 mm. Images are representative of two experiments. **f**, CD69 expression on αCD8^{D-1}-PsT- and αCD8^{D-2}-FITC-stained CD8$^+$ T cells that were uncaged in Ag$^+$ or Ag$^-$ tumor-cell islands. Top: histograms showing CD69 expression on uncaged CD8$^+$ T cells from Ag$^+$ (blue) or Ag$^-$ (red) tumor islands. Bottom: histogram of CD69 expression on uncaged CD8$^+$ T cells from control cultures that only contained Ag$^+$ tumor cells (blue) or Ag$^-$ cells (red). **g**, Quantification of αCD69 fluorescence intensity on αCD8^{D-1}-PsT-labeled CD8$^+$ T cells uncaged in Ag$^+$ or Ag$^-$ regions (as shown in Fig. 3f), analyzed by flow cytometry (for the island cultures $n = 3$ and for the control cultures $n = 1$ technical replicates per group). Representative data from two independent experiments are presented as mean values + s.d. MFI, mean fluorescence intensity.

increased expression in the T-act CD8⁺ T-cell population (Fig. 5b). We then established a gene module containing genes with an expression pattern that was strongly correlated to that of *IFNG*, the most variable gene in the dataset (Extended Data Fig. 7f). As a control, gene correlations to the alternate anchor genes *CCL4* and *CXCL8* resulted in very similar gene lists (Extended Data Fig. 7g). Notably,

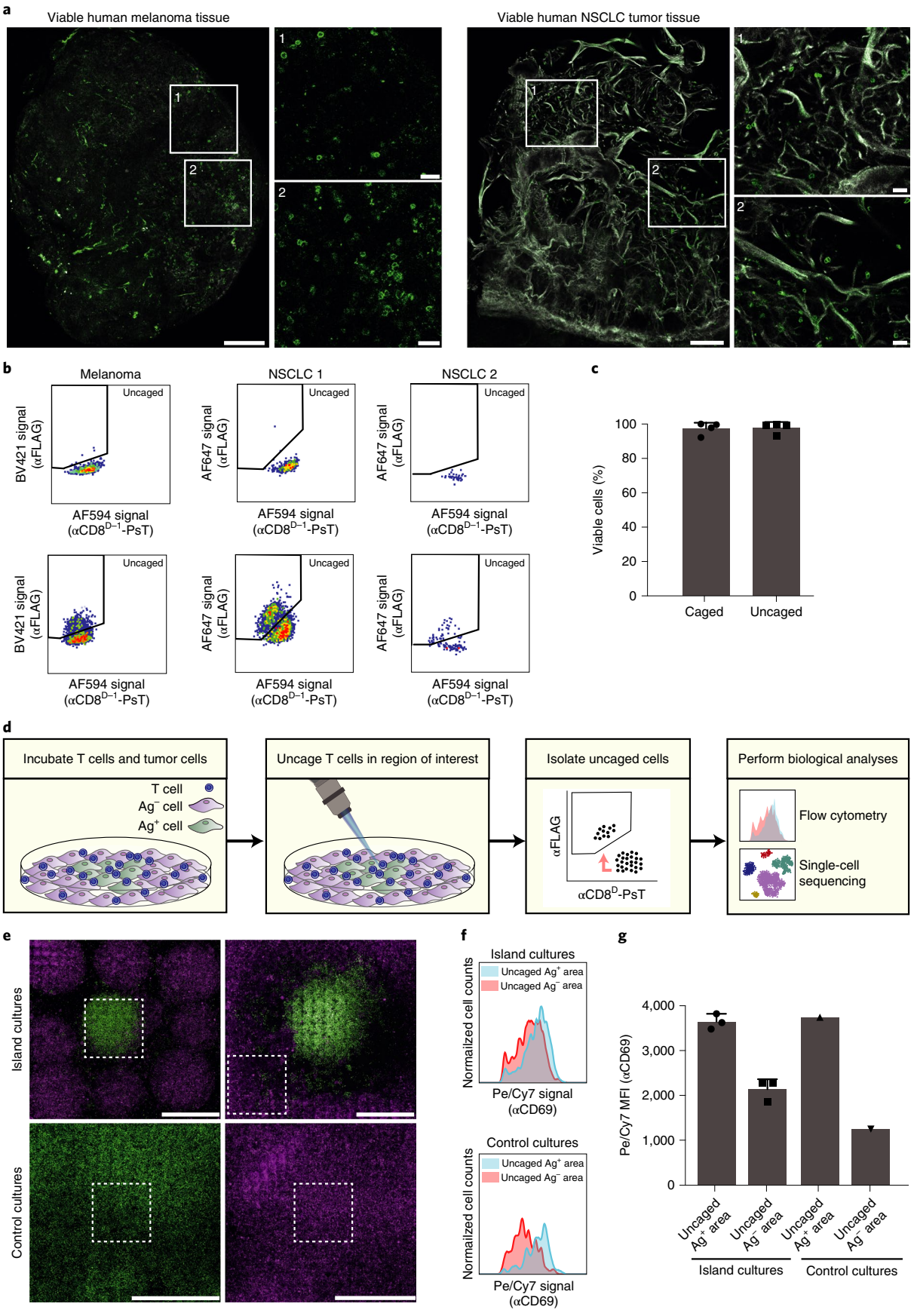

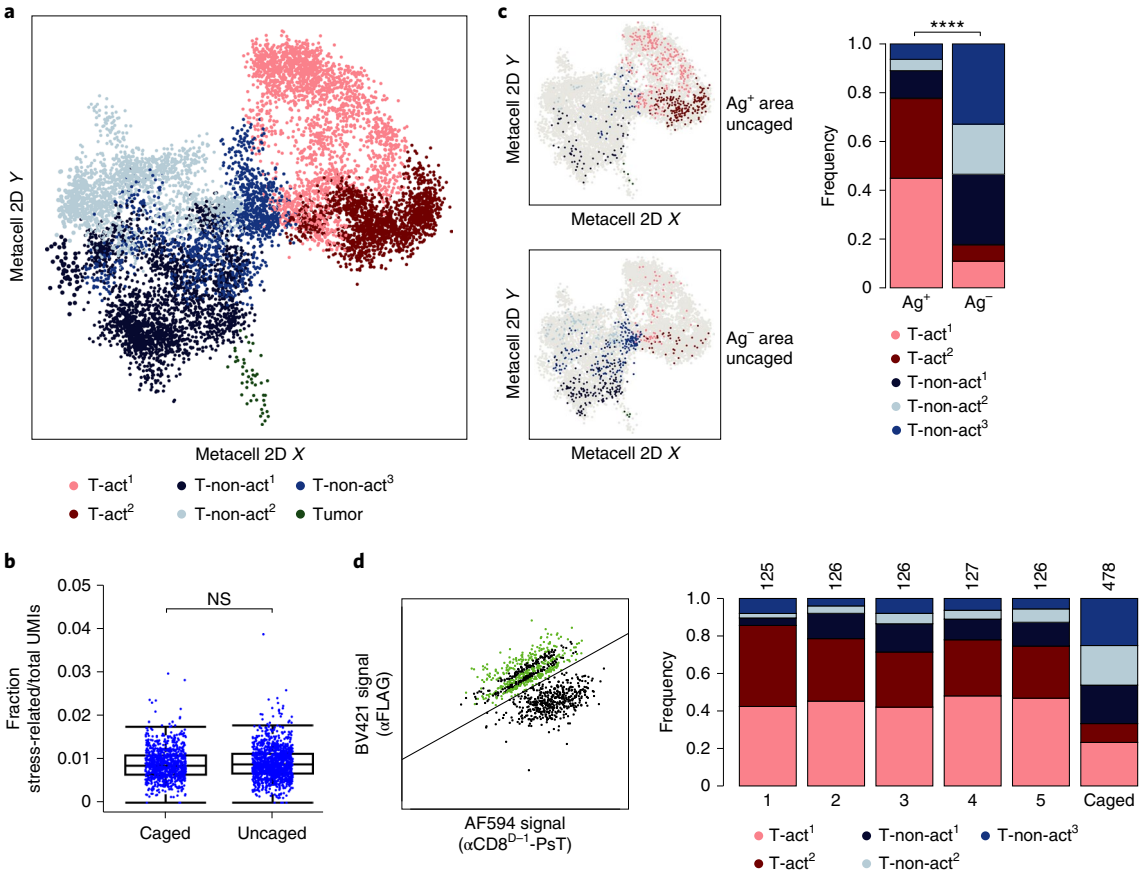

Fig. 4 | Single-cell transcriptomics of spatially defined CD8⁺ T cells. a, A 2D projection of the transcriptional relatedness of 9,237 cells on which single-cell mRNA sequencing was performed and that passed filtering. Individual cells are depicted as dots. Main cell groups are annotated by color, with T-act[1] and T-act[2] (red) showing an activated cell state and T-non-act[1-3] (blue) showing a non-activated state. Tumor cells are depicted in green. **b**, Stress gene expression signature in caged and uncaged CD8⁺ T cells derived from tumor-island cultures, shown as the fraction of unique molecular identifiers (UMIs) from stress-related transcripts (Supplementary Data 4) among the total UMIs per cell in uncaged or caged cells. Boxes show the median and 25th and 75th percentiles. Whiskers depict 1.5 × IQR (interquartile range). A two-tailed Mann–Whitney U test was performed (not significant (NS), $P = 0.0586$). Data are representative of two independent experiments. **c**, Quantification of T-cell states of uncaged CD8⁺ T cells from Ag⁺ and Ag⁻ areas. Plots depict 2D projections of uncaged cells from Ag⁺ (top) or Ag⁻ (bottom) areas, with cells from other conditions depicted in gray. Cells from uncaged areas are colored by their cell states as defined in Fig. 4a and Extended data Fig. 7a,b. Bar plots show the quantification of cell states that are present in the uncaged (AF594^{low} αFLAG^{high}) CD8⁺ T-cell populations from samples in which either Ag⁺ or Ag⁻ areas were uncaged (630 and 615 cells, respectively). Tumor cells are excluded from the bar plots. A two-tailed chi-square test was performed (****$P < 1 \times 10^{-15}$). Data are representative of two independent experiments. **d**, Quantification of the cell states of CD8⁺ T cells showing different levels of uncaging. CD8⁺ T cells from Ag⁺ areas that show varying degrees of uncaging, based on AF594 and αFLAG signals, were divided into five bins containing 127 cells each (shown in alternating green and black), based on their distance from the cutoff line that distinguishes uncaged from caged cells (left). Bin 1 contains cells furthest from the cutoff and bin 5 contains cells closest to the cutoff. Tumor cells were excluded from analysis. Data are representative of two independent experiments.

CD8⁺ T cells that were uncaged in Ag⁺ regions showed increased expression of the *IFNG* module as compared to caged cells (that is, cells from Ag⁻ areas) from the same tumor-island culture (Fig. 5c). Similarly, expression of the *IFNG* module was significantly higher in AF594^{low} αFLAG^{high} CD8⁺ T cells that were derived from uncaged Ag⁺ regions, as compared to AF594^{low} αFLAG^{high} CD8⁺ T cells derived from uncaged Ag⁻ regions (Fig. 5d). Differential gene analysis of uncaged cells from Ag⁺ areas and uncaged cells from Ag⁻ areas confirmed the enrichment of soluble mediator genes as well as activation marker genes in the former cell population (Extended Data Fig. 7g,i). These data demonstrate that location-dependent transcriptional differences can be readily revealed at the gene level. Differences in cell states could also be identified in more complex systems containing many distinct adjacent cell populations, as shown by analysis of T cells co-cultured with a large number of intermingled areas of Ag⁺ and Ag⁻ tumor cells (Extended Data Fig. 8a,b). Finally, we explored the possibility of performing multiplexed analysis of cells residing in distinct regions of the same cell culture. To this end, we set up a strategy involving subsequent rounds of uncaging and in situ labeling with αFLAG antibodies conjugated to distinct fluorochromes, thereby providing cells that are uncaged in different areas with distinct marks (Extended Data Fig. 9a,b). Analysis of the resulting cell pools revealed that cell populations uncaged in subsequent rounds, and hence derived from separate areas, could be readily distinguished (Extended Data Fig. 9c), enabling the direct comparison of transcriptional profiles of cells residing in different areas of the same tissue.

Discussion

The activation and differentiation state of immune cells and other cells are critically dependent on their interaction with environmental signals. For example, recent data demonstrate that differences in the genetic make-up of distinct areas within individual human tumors coincide with variability in the immune infiltrate of these areas[36].

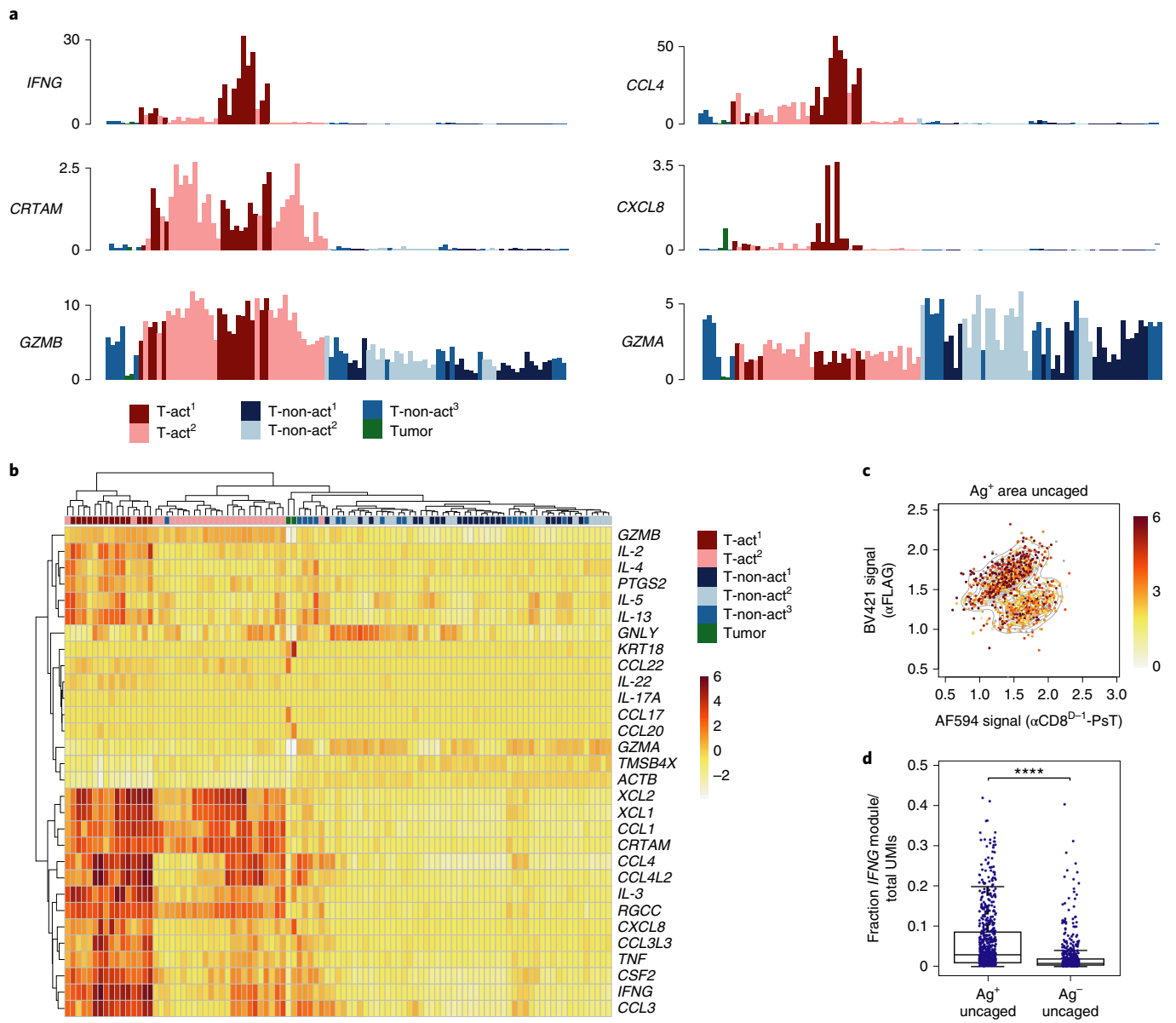

Fig. 5 | Detection of diverse activation programs in locally activated CD8⁺ T cells. a, Bar plots showing the expression levels (transcripts per 1,000 UMIs) of six of the top variable genes throughout the dataset (that is, all cells from all experiments) across all metacells. For each metacell, the mean number of UMIs across cells is depicted. Bars are colored by the cell state annotations used in Fig. 4a. **b**, Heatmap depicting the log fold change in expression relative to the median expression for the top 30 most variable genes in the dataset across all metacells. **c**, Expression of the *IFNG* module per cell in a sample in which αCD8^{D-1}-PsT-labeled CD8⁺ T cells in Ag⁺ areas were uncaged. The color gradient depicts the fraction of UMIs from the *IFNG* module as total UMI count per cell divided by the median fraction of *IFNG* module-related UMIs over all cells. Values were transformed for visualization purposes and are projected on the index plot of the sample in which the Ag⁺ area was uncaged (same index plot as in Extended Data Fig. 7, left). Note that expression of the *IFNG* module is more profound in AF594^{low} αFLAG^{high} CD8⁺ T cells relative to AF594^{high} αFLAG^{low} CD8⁺ T cells from the same sample. Data are representative of two independent experiments. **d**, Expression of the *IFNG* module in spatially defined CD8⁺ T cells. The fraction of UMIs from the *IFNG* module as total UMI count per cell are depicted for uncaged (AF594^{low} αFLAG^{high}) CD8⁺ T cells from samples in which uncaging was either restricted to Ag⁺ areas or Ag⁻ areas. Boxes show the median and 25th and 75th percentiles. Whiskers depict 1.5×IQR and circles depict outlier cells. A two-tailed Mann–Whitney U test was performed (****$P < 1\times10^{-15}$). Data are representative of two independent experiments.

In other words, within human tumors, the local microenvironment is shaped by cellular interactions, either involving direct cell–cell contact or soluble mediators. To dissect how cell states are influenced by the local microenvironment, we developed a small-protein-based photo-uncaging technology that allows the selective isolation of cells from regions of interest in human primary tissue and that enables analysis of single-cell transcriptomes without detectable induction of stress signatures or cell toxicity. The photo-uncaging techniques described in the present work and in the recent work presenting ZipSeq technology[13] share two main advantages as compared to slide-based transcriptomics technologies[6–12]. First, because these approaches allow isolation of viable cells from defined sites, downstream analyses are not restricted to transcriptional or epigenetic profiling, but can also include analysis of functional properties, such as T-cell antigen specificity. Second, while rare cell types and cell states may be missed using grid-based approaches that do not

provide full separation between neighboring cells[6–8], the current approaches do provide information that is unambiguously derived from single-cell units. Of note, photo-uncaging methods do require tissue dissociation for the analysis of cells. Although such tissue dissociation is a common step in single-cell transcriptomics, this may preclude the use of photo-uncaging methods in settings in which only fixed tissue is available.

Although our method and the ZipSeq method[13] share a similar strategy to analyze cells in their environmental context, the two methods exhibit unique strengths. While our photosensitive tag can be used for the uncaging of multiple areas in the same tissue using sequential rounds of uncaging (Extended Data Fig. 9a–c), the use of caged DNA barcodes probably allows a higher degree of multiplexing. On the other hand, the current data establish that SCARI can be used effectively to achieve the isolation of specifically uncaged cells from tissue structures as small as 30–60 cells, whereas such data are not available for ZipSeq. Furthermore, uncaging of the NPBF chromophore as used in SCARI can be performed using low-intensity violet light, rather than the possibly phototoxic ultraviolet light that is generally used to uncage photolabile groups[37]. This makes SCARI of particular interest for the analysis of sensitive cell types and tissues. Finally, the sensitivity of the NPBF cage to two-photon excitation[22] and the simultaneous gain and loss of signals achieved upon uncaging will both be helpful to allow selective marking and isolation of cells located more deeply in live tissues. Although we have here focused on site-specific uncaging of $CD8^+$ T cells, exploiting nanobodies that stably bind to other cell markers (including HLA class I) is also feasible. Using such a pan-cell marker makes it possible to identify cell types that reside in or around specific tumor structures, such as high endothelial venules or tertiary lymphoid structures[38]. Collectively, technologies such as SCARI should contribute to a further understanding of the relationship between cellular location and cell state in human tissues.

Online content

Any methods, additional references, Nature Research reporting summaries, source data, extended data, supplementary information, acknowledgements, peer review information; details of author contributions and competing interests; and statements of data and code availability are available at https://doi.org/10.1038/s41589-021-00839-x.

Received: 3 September 2020; Accepted: 24 June 2021;
Published online: 9 September 2021

References

1. Thommen, D. S. & Schumacher, T. N. T-cell dysfunction in cancer. *Cancer Cell* **33**, 547–562 (2018).
2. Giesen, C. et al. Highly multiplexed imaging of tumor tissues with subcellular resolution by mass cytometry. *Nat. Methods* **11**, 417–422 (2014).
3. Keren, L. et al. MIBI-TOF: a multiplexed imaging platform relates cellular phenotypes and tissue structure. *Sci. Adv.* **5**, eaax5851 (2019).
4. Goltsev, Y. et al. Deep profiling of mouse splenic architecture with CODEX multiplexed imaging. *Cell* **174**, 968–981 (2018).
5. Medaglia, C. et al. Spatial reconstruction of immune niches by combining photoactivatable reporters and scRNA-seq. *Science* **358**, 1622–1626 (2017).
6. Rodriques, S. G. et al. Slide-seq: a scalable technology for measuring genome-wide expression at high spatial resolution. *Science* **363**, 1463–1467 (2019).
7. Moncada, R. et al. Integrating microarray-based spatial transcriptomics and single-cell RNA-seq reveals tissue architecture in pancreatic ductal adenocarcinomas. *Nat. Biotechnol.* **38**, 333–342 (2020).
8. Vickovic, S. et al. High-definition spatial transcriptomics for in situ tissue profiling. *Nat. Methods* **16**, 987–990 (2019).
9. Thrane, K., Eriksson, H., Maaskola, J., Hansson, J. & Lundeberg, J. Spatially resolved transcriptomics enables dissection of genetic heterogeneity in stage III cutaneous malignant melanoma. *Cancer Res.* **78**, 5970–5979 (2018).
10. Ståhl, P. L. et al. Visualization and analysis of gene expression in tissue sections by spatial transcriptomics. *Science* **353**, 78–82 (2016).
11. Berglund, E. et al. Spatial maps of prostate cancer transcriptomes reveal an unexplored landscape of heterogeneity. *Nat. Commun.* **9**, 2419 (2018).
12. Maniatis, S. et al. Spatiotemporal dynamics of molecular pathology in amyotrophic lateral sclerosis. *Science* **364**, 89–93 (2019).
13. Hu, K. H. et al. ZipSeq: barcoding for real-time mapping of single cell transcriptomes. *Nat. Methods* **17**, 833–843 (2020).
14. Sanchez, E. & Huse, M. Spatial and temporal control of T-cell activation using a photoactivatable agonist. *J. Vis. Exp.* **2018**, 56655 (2018).
15. Mayer, G. & Hechel, A. Biologically active molecules with a 'light switch'. *Angew. Chem. Int. Ed.* **45**, 4900–4921 (2006).
16. Klán, P. et al. Photoremovable protecting groups in chemistry and biology: reaction mechanisms and efficacy. *Chem. Rev.* **113**, 119–191 (2013).
17. Yu, H., Li, J., Wu, D., Qiu, Z. & Zhang, Y. Chemistry and biological applications of photo-labile organic molecules. *Chem. Soc. Rev.* **39**, 464–473 (2010).
18. Lee, H. M., Larson, D. R. & Lawrence, D. S. Illuminating the chemistry of life: design, synthesis and applications of 'caged' and related photoresponsive compounds. *ACS Chem. Biol.* **4**, 409–427 (2009).
19. Icha, J., Weber, M., Waters, J. C. & Norden, C. Phototoxicity in live fluorescence microscopy, and how to avoid it. *BioEssays* **39**, 1700003 (2017).
20. Lusic, H. & Deiters, A. A new photocaging group for aromatic N-heterocycles. *Synthesis* **2006**, 2147–2150 (2006).
21. Young, D. D. & Deiters, A. Photochemical hammerhead ribozyme activation. *Bioorg. Med. Chem. Lett.* **16**, 2658–2661 (2006).
22. Komori, N. et al. Design and synthesis of a new chromophore, 2-(4-nitrophenyl)benzofuran, for two-photon uncaging using near-IR light. *Chem. Commun.* **52**, 331–334 (2016).
23. Maurits, E. et al. Immunoproteasome inhibitor–doxorubicin conjugates target multiple myeloma cells and release doxorubicin upon low-dose photon irradiation. *J. Am. Chem. Soc.* **142**, 7250–7253 (2020).
24. Guimaraes, C. P. et al. Site-specific C-terminal and internal loop labeling of proteins using sortase-mediated reactions. *Nat. Protoc.* **8**, 1787–1799 (2013).
25. Dorr, B. M., Ham, H. O., An, C., Chaikof, E. L. & Liu, D. R. Reprogramming the specificity of sortase enzymes. *Proc. Natl Acad. Sci. USA* **111**, 13343–13348 (2014).
26. Capasso, S., Mazzarella, L., Sica, F., Zagari, A. & Salvadori, S. Spontaneous cyclization of the aspartic acid side chain to the succinimide derivative. *J. Chem. Soc., Chem. Commun.* **1992**, 919–921 (1992).
27. Johnson, K. Y., Liu, L. & Vincent, T. S. Minimal FLAG sequence useful in the functional epitope tagging of H-ras. *Biotechniques* **32**, 1270–1280 (2002).
28. Einhauer, A. & Jungbauer, A. The FLAGTM peptide, a versatile fusion tag for the purification of recombinant proteins. *J. Biochem. Biophys. Methods* **49**, 455–465 (2001).
29. Vanier, G. S. Microwave-assisted solid-phase peptide synthesis based on the Fmoc protecting group strategy (CEM). *Methods Mol. Biol.* **1047**, 235–249 (2013).
30. Bannas, P. et al. Molecular imaging of tumors with nanobodies and antibodies: timing and dosage are crucial factors for improved in vivo detection. *Contrast Media Mol. Imaging* **10**, 367–378 (2015).
31. Jaitin, D. A. et al. Massively parallel single-cell RNA-seq for marker-free decomposition of tissues into cell types. *Science* **343**, 776–779 (2014).
32. Baran, Y. et al. MetaCell: analysis of single-cell RNA-seq data using *K*-nn graph partitions. *Genome Biol.* **20**, 206 (2019).
33. Ayers, M. et al. IFN-γ-related mRNA profile predicts clinical response to PD-1 blockade. *J. Clin. Invest.* **127**, 2930–2940 (2017).
34. Russo, R. C., Garcia, C. C., Teixeira, M. M. & Amaral, F. A. The CXCL8/IL-8 chemokine family and its receptors in inflammatory diseases. *Expert Rev. Clin. Immunol.* **10**, 593–619 (2014).
35. Repeke, C. E., Garlet, T. P., Fonseca, A. C., Silveira, E. M. & Garlet, G. P. in *Encyclopedia of Signaling Molecules* (ed. Choi, S.) 805–809 (Springer, 2018); https://doi.org/10.1007/978-3-319-67199-4_10
36. Ghorani, E. et al. The T-cell differentiation landscape is shaped by tumour mutations in lung cancer. *Nat. Cancer* **1**, 546–561 (2020).
37. Van De Graaff, M. J. et al. Conditionally controlling human TLR2 activity via *trans*-cyclooctene caged ligands. *Bioconjug. Chem.* **31**, 1685–1692 (2020).
38. Dieu-Nosjean, M. C., Goc, J., Giraldo, N. A., Sautès-Fridman, C. & Fridman, W. H. Tertiary lymphoid structures in cancer and beyond. *Trends Immunol.* **35**, 571–580 (2014).

Methods

Human material. Human tumor tissue was obtained either following an opt-out procedure or upon prior informed consent, in accordance with national guidelines and after approval by the local medical ethical committee (institutional review board) of The Netherlands Cancer Institute. Tumor tissue was collected from surgical specimens after macroscopic examination of the tissue by a pathologist. Tumor tissue was dissected into fragments of 1–2 mm^3 and frozen in 90% fetal calf serum (FCS, Sigma) and 10% dimethyl sulfoxide (DMSO, Sigma). PBMCs were isolated from the blood of healthy donors (Sanquin) using standard Ficoll (GE Healthcare) gradient centrifugation separation. PBMCs were stored in liquid nitrogen in 90% FCS and 10% DMSO until further use.

Production of recombinant nanobodies in *Escherichia coli*. Monomeric and dimeric variants of two human αCD8 nanobody clones ($\alpha CD8^{M}$, $\alpha CD8^{D-1}$ and $\alpha CD8^{D-2}$) and dimeric variants of αHLA class I (specific for the β2M subunit of HLA class I, $\alpha HLA\text{-}I^{D}$) and mouse αCD47 ($\alpha CD47^{D}$) nanobody clones were generated as follows. *E. coli* WK6 cells were transformed with the pHEN6 expression vector (for production of the $\alpha CD8^{M}$ nanobody) and *E. coli* BL21 cells were transformed with the pET22b expression vector (for production of the $\alpha CD8^{D}$, $\alpha HLA\text{-}I^{D}$ and $\alpha CD47^{D}$ nanobodies) encoding the relevant nanobody sequence, followed by an LPETGG-6xH sequence. $\alpha CD8^{D}$ nanobodies were formed by coupling two monomeric αCD8 domains with a flexible GC-rich linker. Protein production was induced with IPTG (Thermo Fisher Scientific) and recombinant proteins were isolated from the periplasmic fraction using Ni-NTA beads (Qiagen). Following washing and subsequent elution with 50 mM Tris (pH 8), 150 mM NaCl and 500 mM imidazole, samples were purified by gel filtration chromatography on a Phenomenex Biosep SEC-S3000 column in phosphate-buffered saline (PBS) and material was concentrated using an Amicon 10-kDa molecular weight cutoff (MWCO) filtration unit (Millipore). Nanobodies were stored at −80 °C until further use.

Labeling of nanobodies with PsT. Maleimide dyes (maleimide-AF647 and maleimide-FITC) were coupled to GGGC peptide by incubation of 1 mg (~20 μg ml^{-1}) of the fluorescent maleimide with 175–200 μM GGGC peptide for a minimum of 2 h at room temperature in 10–12.5 mM $NaHCO_3$. Subsequently, conjugates were purified by reverse-phase HPLC on a C18 column (Waters) and the identity of the obtained material was confirmed by mass spectrometry. The resulting molecules, and the PsT, which also contains a GGGC motif, were coupled to the indicated nanobodies by sortase reactions[39]. In brief, 2.5 μM purified nanobody-LPETGG-6xH protein was incubated with either 40 μM GGGC-dye or 40 μM PsT and 0.4 μM hepta-(7M) mutant sortase for 2 h at 4 °C in 50 mM Tris (pH 8) and 150 mM NaCl. Hepta-(7M) mutant sortase was produced in-house, as described in ref. [40]. Unreacted nanobodies and sortase were removed by adsorption onto Ni-NTA agarose beads (Qiagen). The suspension was then added on top of a 100-kDa cutoff filter to remove the Ni-NTA agarose beads, and the flow-through (containing labeled nanobody and unconjugated GGGC-dye or PsT) was further purified and concentrated. Unconjugated GGGC-dye or PsT was removed using an Amicon 10-kDa MWCO filtration unit (Millipore) and the material was further purified using a Zeba spin column (Thermo Fisher Scientific). To create nanobodies containing a monomeric PsT, PsT-labeled nanobodies were incubated with 5 mM DTT for 30 min at room temperature, followed by addition of 8 mM iodoacetamide for 30 min at room temperature. Reduced nanobody-PsTs were purified using a Zeba spin column and concentrated using an Amicon 10-kDa MWCO filtration unit. Labeled nanobodies were stored in PBS at −20 °C. Protein concentrations were determined by spectrophotometry and individual batches of labeled nanobodies were titrated for optimal usage (with final concentrations ranging from 5 to 10 μg ml^{-1}). The purity of unlabeled and PsT-labeled nanobodies were assessed using a NuPAGE 4–12% Bis-Tris gel (Thermo Fisher Scientific) and InstantBlue Protein Stain (Novus Biologicals). Protein Stain and fluorescence signals were measured with a Typhoon FLA 9500 laser scanner.

Cell lines and tissue preparations. $CD8^+$ T cells were isolated from PBMCs using a $CD8^+$ T-cell Isolation Kit (Miltenyi Biotec). PBMCs and $CD8^+$ T cells were cultured in RPMI medium (Gibco) supplemented with 10% human serum (Sigma), penicillin (100 U ml^{-1}, Roche), streptomycin (100 μg ml^{-1}, Roche) and recombinant human interleukin-2 (hIL-2) (60 IU ml^{-1}, Novartis). BA/F3 cells (kindly provided by J. Leusen, UMC Utrecht, Netherlands[41]) were cultured in RPMI supplemented with 10% FCS, penicillin (100 U ml^{-1}), streptomycin (100 μg ml^{-1}) and 0.2 ng ml^{-1} mouse IL-3 (Immunotools). OVCAR5 cells (kindly provided by F. Scheeren, The Netherlands Cancer Institute, Netherlands) were cultured in Iscove's Modified Dulbecco's Medium IMDM (Gibco) supplemented with 10% FCS, penicillin (100 μg ml^{-1}), streptomycin (100 μg ml^{-1}) and GlutaMax (1×, Gibco). Viable human tumor tissue pieces (~1–2 mm^3) were thawed in prewarmed DMEM (Gibco) supplemented with 10% FCS, penicillin (100 U ml^{-1}), streptomycin (100 μg ml^{-1}), sodium pyruvate (1 mM, Sigma), MEM non-essential amino acids (1×, Sigma) and GlutaMax (1×). Tumor tissue was subsequently washed three times by thoroughly submerging and shaking the tissue pieces in fresh prewarmed medium.

Viral transduction of tumor cells and T cells. $CDK4_{R>L}^+$ GFP^+ OVCAR5 cells (Ag^+ tumor cells), $Katushka^+$ OVCAR5 cells (Ag^- tumor cells) and IFN-$\gamma R^{-/-}$ OVCAR5 cells (see below) were generated as described previously[42]. $CDK4_{R>L}$-specific $CD8^+$ T cells were generated[42,43] and expanded[44] as described previously. Upon recognition of Ag^+ tumor cells, $CDK4_{R>L}$-specific $CD8^+$ T cells are activated.

Analysis of nanobody binding stability. $CD8^+$ T cells were stained with either $\alpha CD8^{M}$, $\alpha CD8^{D-1}$ or $\alpha CD8^{D-2}$ (FITC or AF647 labeled), as indicated in Extended Data Fig. 2a,b, in PBS supplemented with 0.5% bovine serum albumin (BSA, Sigma) and EDTA (2 mM, Life Technologies) for 30 min at 4 °C. After three washes with PBS containing 0.5% BSA and EDTA, stained $CD8^+$ T cells were mixed as indicated, followed by a 30-min incubation at 37 °C in RPMI with penicillin, streptomycin and 10% human serum. Afterwards, cells were resuspended in PBS with 0.5% BSA and EDTA (2 mM) and analyzed by flow cytometry.

Staining of cells and tissues before uncaging. Where indicated, human $CD8^+$ T cells, PBMCs and tumor tissue were stained with $\alpha CD8^{D-1}$-PsT or $\alpha HLA\text{-}I^{D}$-PsT and $\alpha CD8^{D-2}$ (FITC or AF647, serving as a stable signal to identify cells after loss of the AF594-positive cage) in PBS supplemented with 0.5% BSA and EDTA (2 mM) for 30 min at 4 °C while gently shaking. Where mixing of cells from exposed and non-exposed samples was indicated, exposed cells were additionally stained with αCD3-FITC (SK7, BD Biosciences, 1:30) and non-exposed cells were stained with either αCD3-BV711 (UCHT1, BD Biosciences, 1:100) or αCD3-APC (SK7, BD Biosciences, 1:30) to allow distinction between cells from exposed and non-exposed samples. BA/F3 cells were stained with mouse $\alpha CD47^{D}$-PsT and αCD44-AF647 antibody (IM7, Biolegend, 1:50, serving as a stable marker) in PBS with 0.5% BSA and EDTA for 30 min at 4 °C. Cells and tumor tissue were washed and taken up in PBS supplemented with 0.5% BSA and EDTA for confocal microscopy. For staining of OVCAR5 cells for multiplex experiments, see section 'Multiplexed uncaging of tumor islands'. Where indicated, the reduced version of PsT-labeled nanobodies, containing a monomeric PsT, was used.

Tumor cell–T cell cultures. Three to five days before co-culture, tumor cells were plated in small droplets (±5,000 cells per 5-μl droplet) on polymer or glass bottom eight-well μ-slides (Ibidi) in IMDM medium supplemented with 8% FCS, penicillin (100 U ml^{-1}), streptomycin (100 μg ml^{-1}) and GlutaMax (1×). Ag^+ GFP^+ and Ag^- $Katushka^+$ tumor cells were plated as indicated per experiment. Following tumor cell adherence, remaining non-adherent cells were removed by washing and cells were cultured in IMDM with 8% FCS, penicillin, streptomycin and GlutaMax. Subsequently, $\alpha CD8^{D-1}$-PsT- and $\alpha CD8^{D-2}$-FITC-stained $CDK4_{R>L}$ TCR^+ $CD8^+$ T cells were added, and cells were cultured for 4 h at 37 °C in the climate chamber of a Leica SP8 Confocal system (Leica Microsystems) microscope, as discussed in the next section.

Confocal microscopy imaging and local uncaging. All images were acquired using an inverted Leica SP8 Confocal system equipped with four tunable hybrid detectors, visible lasers (405-nm argon, DPSS 561 nm and HeNe 633 nm) and an Insight X3 multi-photon laser (Spectra Physics). All images were collected at 12 bit and acquired with a ×25 water immersion objective with a free working distance of 2.40 mm (HC FLUOTAR L ×25/0.95 W VISIR 0.17). Fluorophores were excited as follows: FITC and GFP at 488 nm, AF594 and Katushka at 561 nm and AF647 at 633 nm. The FITC and GFP signals were collected between 510 and 590 nm, the AF594 signal between 610 and 650 nm, the Katushka signal between 620 and 720 nm and the AF647 signal between 680 and 750 nm. $CD8^+$ T cells, PBMCs and BA/F3 cells were seeded in a Micro-Insert four-well u-Dish (Ibidi) and placed onto the microscope with a climate chamber adjusted to 37 °C. Similarly, multiplexing cultures and tumor cell–T cell co-cultures were imaged and incubated in eight-well μ-slides in the climate chamber at 37 °C. Overview scans of the entire well were acquired. Tumor tissue was placed between two cover slips (Duran) and kept ice-cold using custom-made cool packs during image acquisition. Both overview scans and 3D tile scans of the entire tumor fragments (with Z-step size of 1 μm) were acquired. Note that, in tumor tissues, the $\alpha CD8^{D-2}$-FITC signal is predominantly detected, so, although also stained with $\alpha CD8^{D-1}$-PsT (AF594), $CD8^+$ T cells are depicted in green in microscopy images.

To uncage the $\alpha CD8^{D-1}$-PsT, $\alpha\beta 2M^{D}$-PsT and $\alpha CD47^{D}$-PsT in defined areas, a population of cells was selected by drawing a region of interest. For each defined region of interest, a Z-stack was made with step sizes of 1 μm. Unless indicated otherwise, uncaging was performed using the 405-nm laser line at 15% power (equivalent to 865 μW mm^{-2}), 600 Hz, ×25 magnification and 1,024 × 1,024 pixels, with a pixel dwell time of 600 ns. For the experiments testing the resolution of SCARI (Fig. 2d–f), zoom (ranging from ×1 to ×16) and number of pixels (ranging from 1,024 × 1,024 to 64 × 64 pixels per uncaging field) were adjusted to keep the laser exposure comparable between conditions.

Collection and dissociation of cells and tumor tissue. $CD8^+$ T cells, PBMCs and BA/F3 cells were collected by resuspension. Adherent cells were trypsinized with PBS supplemented with trypsin-EDTA (1×, Thermo Fisher Scientific) at 37 °C and collected cell fractions were pooled for subsequent staining steps in the case of tumor cell–T cell co-cultures. Tumor tissue was dissociated by incubation with collagenase IV (1 mg ml^{-1}, Sigma-Aldrich) and pulmozyme (12.5 μg ml^{-1}, Roche) in

RPMI for 20 min at 37 °C. After dissociation, tumor-cell suspensions were filtered through a 35-µm cell strainer (Falcon tube with cell strainer cap, Corning) and washed with cold PBS supplemented with 0.5% BSA and EDTA (2 mM).

αFLAG staining of cell suspensions after uncaging. Where indicated, PBMCs, BA/F3 cells, CD8$^+$ T cells, dissociated tumor tissue and T cell–tumor cell suspensions were stained in cold PBS with 0.5% BSA and EDTA (2 mM) for 20–30 min at 4 °C with the following: live–dead fixable near-IR dead cell stain (IR-dye, Thermo Fisher Scientific), αCD3-BV711 antibody and αFLAG-AF647 antibody (D6W5B, Cell Signaling Technology, 1:50), polyclonal αFLAG-AF647 (Cell Signaling Technology, 1:200), αFLAG-BV421 (L5, Biolegend, 1:50) or primary unlabeled αFLAG antibody (D6W5B, Cell Signaling Technology, 1:800), followed by secondary αRabbit-IgG-BV421 antibody (BD Biosciences, 1:200). In tumor–T cell co-culture experiments, cells were also stained with αCD69-PeCy7 (H57-597, Biolegend, 1:100). Following staining, cells were washed three times and resuspended in cold PBS with 0.5% BSA and EDTA (2 mM) for flow cytometry.

Multiplexed uncaging of tumor islands. Tumor islands containing either GFP$^+$ OVCAR5 cells or IFN-γR$^{-/-}$ OVCAR5 cells (to distinguish the two cell populations in flow cytometry based on GFP and IFN-γR signals) were generated as discussed above. Plated GFP$^+$ and IFN-γR$^{-/-}$ OVCAR5 cells were stained with αHLA-I^{D}-PsT and αHLA-A2-FITC (BB7.2, BD Biosciences, 1:50, serving as stable membrane markers) in IMDM with 8% FCS, penicillin, streptomycin and GlutaMax for 30 min at 37 °C. After the cells were washed with IMDM with 8% FCS, penicillin, streptomycin and GlutaMax, cells were covered in PBS supplemented with 8% FCS for confocal microscopy. In a first uncaging round, cells located in a GFP$^+$ tumor island were uncaged following the uncaging procedure described above, and cells were subsequently stained with αFLAG-AF647 (D6W5B) (αFLAG^1) for 30 min in the climate chamber of the Leica SP8 Confocal system at 37 °C. Cells were then washed with IMDM with 8% FCS, penicillin, streptomycin and GlutaMax, and covered in PBS with 8% FCS. Next, in a second uncaging round, cells located in an IFN-γR$^{-/-}$ cell island were uncaged, followed by trypsinization of cells with PBS supplemented with trypsin-EDTA for 4 min at 37 °C. After trypsinization, tumor cells were stained with αIFN-γR1 antibody (GIR-208; eBioscience, 1:50, to distinguish GFP$^+$ IFN-γR-proficient cells from membrane-stained IFN-γR$^{-/-}$ cells) and primary unlabeled αFLAG antibody (D6W5B) (αFLAG^2) followed by secondary αRabbit-IgG-BV421 antibody (BD Biosciences) and IR-dye. Following staining, cells were washed three times and resuspended in cold PBS with 0.5% BSA and EDTA (2 mM), then analyzed by flow cytometry.

Single-cell sorting of CD8$^+$ T cells. CD8$^+$ T cells were single-cell sorted based on the following gating strategy. Forward and sideward scatter were used to exclude doublets and to distinguish CD8$^+$ T cells from tumor cells. Viable CD8$^+$ T cells were identified by the expression of CD3, CD8 (as reflected by staining with αCD8^{D-1}-PsT and αCD8^{D-2}-FITC) and a low IR-dye signal. CD69 expression was also measured. For each sample, uncaged CD8$^+$ T cells (AF594^{low} αFLAG^{high}) and total CD8$^+$ T cells were sorted using index sorting into 384-well plates containing 2 µl of lysis solution with barcoded poly(T) reverse-transcription (RT) primers (IDT[45]) per well. Four wells were left empty in each 384-well plate to be used as background controls in single-cell sequencing. Following cell sorting, plates were briefly centrifuged, snap-frozen on dry ice and stored at −80 °C.

Single-cell library preparation. Single-cell libraries were prepared as described previously using MARS-seq[31]. In brief, following single-cell sorting and cell lysis in 384-well capture plates, mRNA was barcoded and converted into cDNA. cDNA was pooled using an automated pipeline and the pooled sample was linearly amplified by T7 in vitro transcription. The resulting RNA was fragmented and converted into a sequencing-ready library by tagging the samples with pool barcodes and Illumina sequences during ligation, reverse transcription and polymerase chain reaction. For each pool of cells, both library quality and library concentration were assessed.

MARS-seq data processing. Sequencing of single-cell RNA-sequencing libraries pooled at equimolar concentration was performed on a NextSeq 500 system (Illumina) with a median sequencing depth of ~40,000 reads per cell. Sequences were mapped to the human genome (hg19), demultiplexed and filtered as described in ref. [31], with the modifications reported in ref. [45].

Metacell modeling and analysis. For modeling of single-cell RNA-sequencing data, we used the MetaCell package version 3.41[32], using a similar strategy as described in ref. [45]. In brief, sets of mitochondrial genes, immunoglobulin genes, ribosomal protein genes and long noncoding RNA genes (Supplementary Data 3) were removed. Cells with fewer than 500 unique molecular identifiers (UMIs) were filtered out, as well as cells with a fraction of mitochondrial gene expression that exceeded 0.6. Feature genes were selected using a threshold value for the normalized var/mean (Tvm) of 0.08 and total UMI count of 100. Gene features that were associated with lateral processes, such as cell cycle, type I IFN response or stress (adapted from ref. [45], Supplementary Data 4), were excluded from metacell formation.

Metacell generation was performed on 9,237 cells using 444 genes that passed the filtering steps. $K = 100$ and 500 bootstrap iteration steps were performed and heterogeneous metacells were split. The metacell confusion matrix was used to annotate groups of metacells that showed similar expression profiles. Three main cell groups (activated CD8$^+$ T cells, non-activated CD8$^+$ T cells and tumor cells) were classified based on the expression of marker genes. Tumor cells were excluded from further analysis where indicated. Supervised analysis of cell states was performed as described in the main text.

Cell state analysis of uncaged cells. To annotate single cells as caged or uncaged, mean fluorescence intensity values of the αCD8^{D-1}-PsT and αFLAG signals per cell were used and defined as above cutoff (AF594^{low} αFLAG^{high}; uncaged) or below cutoff (AF594^{high} αFLAG^{low}; caged). To analyze the states of CD8$^+$ T cells with different levels of uncaging, the total uncaged population was divided into five bins containing equal numbers of cells (before exclusion of tumor cells), based on their distance from the cutoff line between the uncaged and caged populations, with bin 1 containing cells with the highest level of uncaging and bin 5 containing cells that were closest to the cutoff. For subsequent analysis of T-cell states per bin, tumor cells were excluded.

The most variable genes within the dataset were defined based on their variance over all cells divided by the mean. To generate gene modules that were associated with the expression of the most variable genes, we identified the top 30 genes that correlated to one of the indicated anchor genes, *IFNG*, *CCL4* and *CXCL8*, using a linear correlation of the log fold change of the expression value of a gene in each metacell over the median expression value over all metacells. Genes that were part of the cell cycle, type I IFN response or stress modules were excluded from this analysis. The expression of gene signatures ('signature score') for both the stress gene module and the *IFNG* gene module was plotted as the fraction of signature-related UMIs of total UMIs per cell.

Software. For acquisition of microscopic images in this study, LASX 3.5.5 was used. Flow cytometry data acquisition and analysis were done using FACS Diva 7 and FlowJo 10.6.2. Statistical analyses were performed in Prism (GraphPad) 8.0.0. Analysis of single-cell RNA-sequencing data was carried out using R 3.6.2 and RStudio 1.2.1335.

Reporting Summary. Further information on research design is available in the Nature Research Reporting Summary linked to this Article.

Data availability

The processed single-cell RNA-sequencing data are deposited in the NCBI Gene Expression Omnibus (GEO) under accession no. GSE175813. Source data are provided with this paper.

Code availability

The code reproducing the analyses in this study is available as a supplementary file to NCBI GEO accession no. GSE175813.

References

39. Antos, J. M. et al. Site-specific protein labeling via sortase-mediated transpeptidation. *Curr. Protoc. Protein Sci.* **89**, 15.3.1–15.3.19 (2017).
40. Dijkgraaf, F. E. et al. Tissue patrol by resident memory CD8$^+$ T cells in human skin. *Nat. Immunol.* **20**, 756–764 (2019).
41. Bracke, M., Lammers, J. W. J., Coffer, P. J. & Koenderman, L. Cytokine-induced inside-out activation of FcαR (CD89) is mediated by a single serine residue (S263) in the intracellular domain of the receptor. *Blood* **97**, 3478–3483 (2001).
42. Hoekstra, M. E. et al. Long-distance modulation of bystander tumor cells by CD8$^+$ T-cell-secreted IFN-γ. *Nat. Cancer* **1**, 291–301 (2020).
43. Van Rooij, N. Tumor exome analysis reveals neoantigen-specific T-cell reactivity in an ipilimumab-responsive melanoma. *J. Clin. Oncol.* **31**, e439–e442 (2013).
44. Linnemann, C. et al. High-throughput identification of antigen-specific TCRs by TCR gene capture. *Nat. Med.* **19**, 1534–1541 (2013).
45. Li, H. et al. Dysfunctional CD8 T cells form a proliferative, dynamically regulated compartment within human melanoma. *Cell* **176**, 775–789 (2019).

Acknowledgements

Plasmid sequences for αCD8 nanobodies were kindly provided by 121Bio with support from M. Gostissa and G. Grotenbreg. We thank H. Ploegh for providing the sortase expression vector. We thank M. Marqvorsen, M. de Weert, M. de Bruijn, K. Bresser, D. Philips, D. Elatmioui, P. Hekking, N. Meeuwenoord, H. van den Elst, B. Florea, L. Bornes and staff of the NKI Flow Cytometry facility for technical support and input, and members of the van Kasteren, van Rheenen and Schumacher laboratories for

discussions. This work was supported by ERC AdG SENSIT grant 742259 to T.N.S. and ERC StG Crosstag grant 639005 and ERC Cog KineTic grant 865175 to S.I.v.K.

Author contributions

A.M.v.d.L., M.E.H., L.R., M.J.v.d.G., S.I.v.K. and T.N.S. conceived the project and contributed to experimental design. A.M.v.d.L., M.E.H., C.L.G.J.S. and M.T. designed, performed and analyzed the biological experiments. C.L.G.J.S. and L.Y.Y.C. performed microscopy experiments. L.R., M.T., M.J.v.d.G. and S.I.v.K. designed, synthesized and validated the photocaged compounds. L.R. and C.L.G.J.S. contributed equally to the execution of the experiments. H.L. performed single-cell sequencing and E.D. performed sequence alignments. A.M.v.d.L. performed computational analysis. H.L., A.B., Y.L. and A.T. provided input on the computational analysis. D.S.T. was responsible for human tumor sample acquisition. A.M.v.d.L., M.E.H., L.R., S.I.v.K. and T.N.S. wrote the manuscript, with input from all other co-authors. J.v.R., I.A., S.I.v.K. and T.N.S. supervised the project.

Competing interests

The authors declare no competing interests.

Additional information

Extended data is available for this paper at https://doi.org/10.1038/s41589-021-00839-x.

Supplementary information The online version contains supplementary material available at https://doi.org/10.1038/s41589-021-00839-x.

Correspondence and requests for materials should be addressed to S.I.v.K. or T.N.S.

Peer review information *Nature Chemical Biology* thanks Johannes Broichhagen and the other, anonymous, reviewer(s) for their contribution to the peer review of this work.

Reprints and permissions information is available at www.nature.com/reprints.

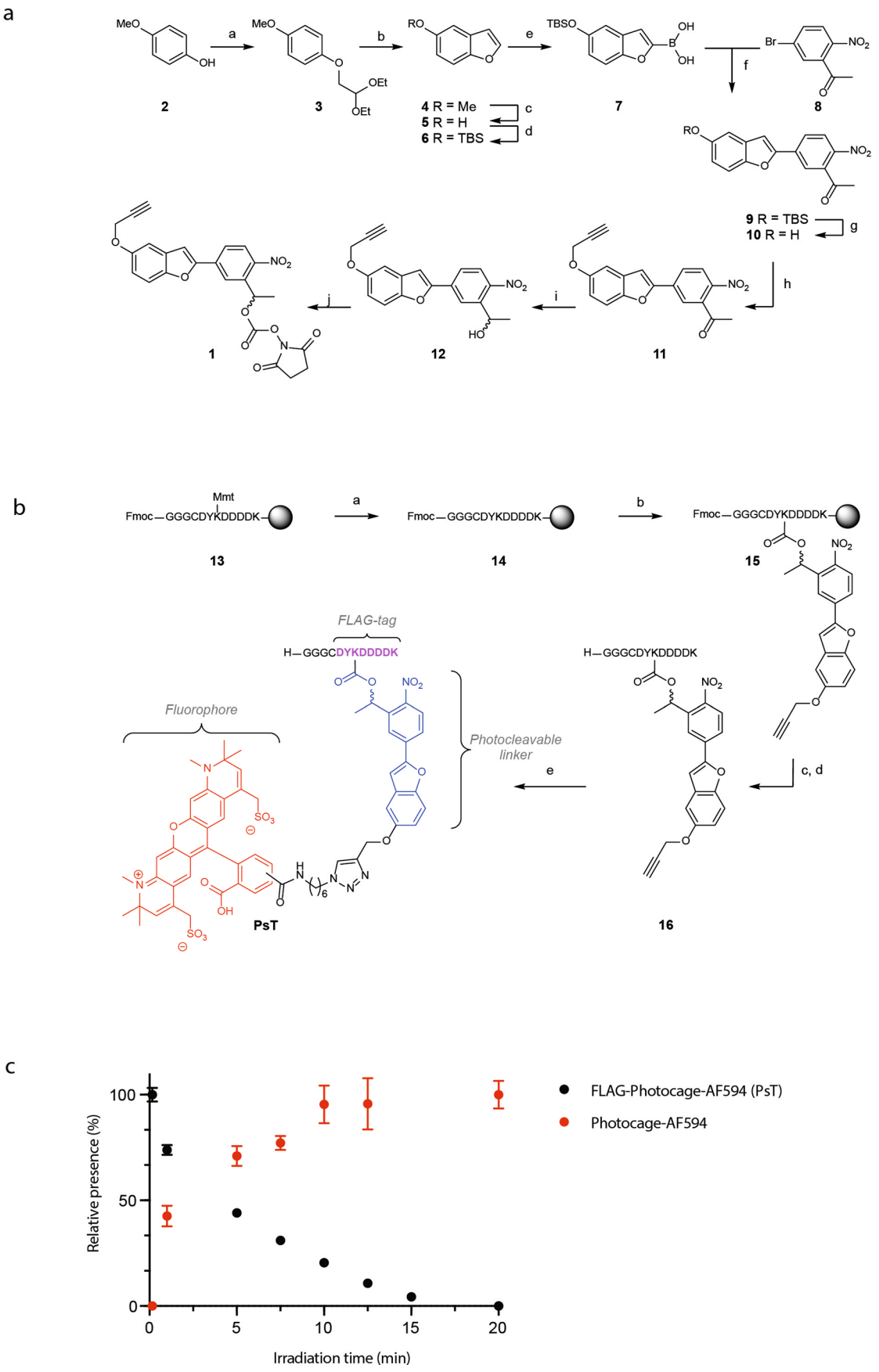

Extended Data Fig. 1 | See next page for caption.

Extended Data Fig. 1 | Synthesis of bis functionalized NPBF based photocleavable linker and the photo-sensitive tag (PsT). (a) Reagents and conditions for synthesis of the NPBF cage: a) bromoacetaldehyde diethyl acetal, KOH, NMP, 70 °C, 15 hours, 90%; b) polyphosphoric acid, toluene, 111 °C, 16 hours, 33%; c) BBr3, DCM, 1 hour at - 78 °C then 1 hour at room temperature, 89%; d) TBDMSCl, imidazole, DMF, 1 hour, room temperature, 70%; e) (i) n-BuLi, THF, -78 °C, 1 hour, (ii) triisopropyl borate, 30 minutes at -78 °C then 30 minutes at room temperature; f) Pd(PPh3)4, K_2CO_3, THF/H2O, 75 °C, 18 hours, 75%; g) HF-pyridine, THF, room temperature, 1 hour, 77%; h) K_2CO_3, propargyl bromide, room temperature, 5 hours, 86%; i) NaBH4, 1,4-dioxane/ methanol, room temperature, 1 hour, 0 °C to room temperature, 88%; j) N,N′-disuccinimidyl carbonate, Et3N, DMF, room temperature, 4 hours, 79%. (b) Reagents and conditions for synthesis of the PsT: a) 1% TFA, DCM, room temperature, 30 minutes (2x); b) 1, DiPEA, DMF, room temperature, 18 hours; c) 20% piperidine, DMF, room temperature, 2 minutes (3x), d) TFA, TIS, H_2O 95/2.5/2.5, room temperature, 3 hours; e) $CuSO_4$, sodium ascorbate, THPTA, AF594-N3, H_2O, t-BuOH room temperature, 2 hours. (c) Uncaging efficiency of the PsT over time. 10μM PsT (in water) was uncaged with 420-nm light using a 1W LED-lamp for the indicated times and reaction products were measured using LC-MS analysis. Data points represent the mean +/- s.d. of technical triplicates (n=3) from a single experiment.

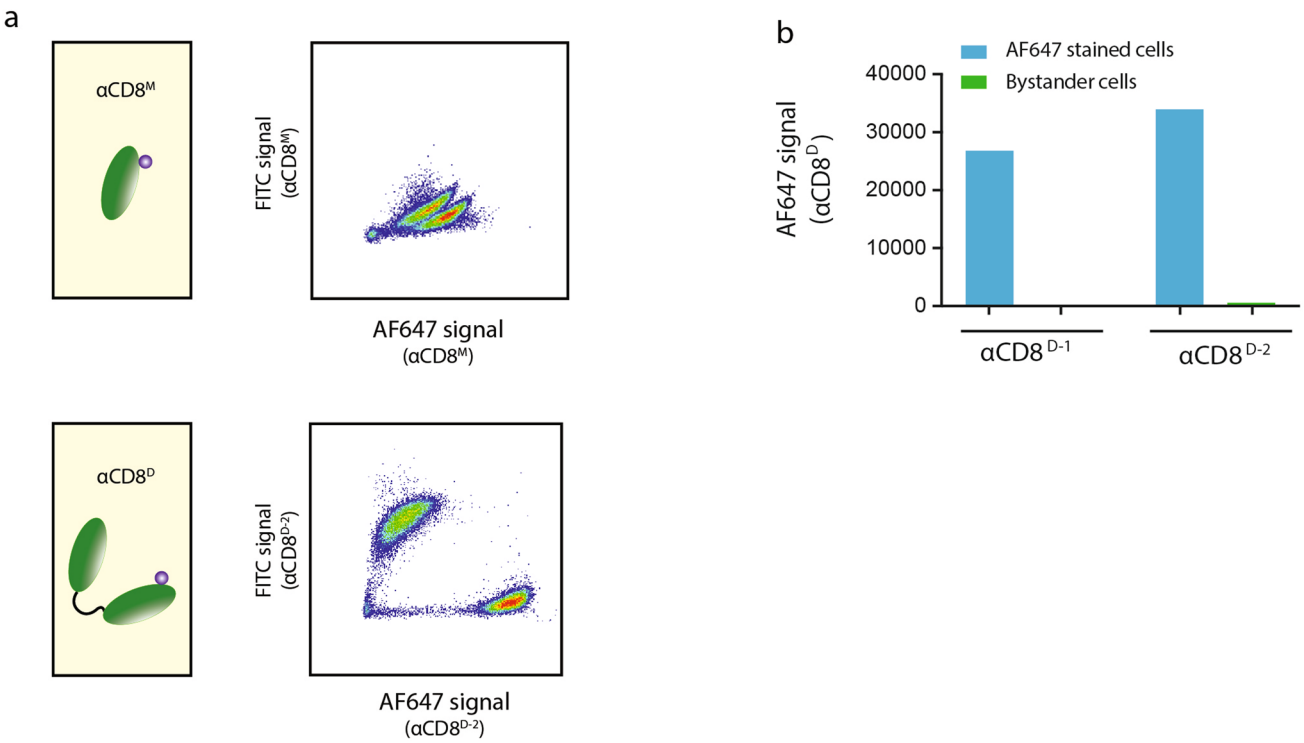

Extended Data Fig. 2 | Generation of stable dimeric αCD8 nanobodies. (**a**) Binding stability of αCD8 nanobodies to CD8⁺ T cells. Top panel: a first population of CD8⁺ T cells was stained with FITC labeled monomeric nanobody (αCD8^{M}-FITC) and a second population was stained with αCD8^{M}-AF647. Bottom panel: a first population of CD8⁺ T cells was stained with FITC labeled dimeric nanobody containing recognition domains that are identical to the αCD8^{M} (αCD8^{D-2}-FITC) and a second population was stained with αCD8^{D-2}-AF647. Subsequently, two cell populations labeled with either monomeric or dimeric αCD8 reagents were mixed, incubated at 37°C, and exchange of αCD8 nanobodies was measured by flow cytometry. Quantification of this αCD8^{D-2} clone and of a second nanobody clone αCD8^{D-1} is depicted in Extended data Fig. 2b. (**b**) Data depict AF647 fluorescence signal of two CD8⁺ T cell populations that were either stained with the indicated αCD8^{D}-AF647 or with the corresponding αCD8^{D}-FITC, and that were mixed and subsequently incubated at 37 °C. Note the lack of substantial AF647 signal on the FITC-labeled bystander pool. Data are representative of 2 independent experiments.

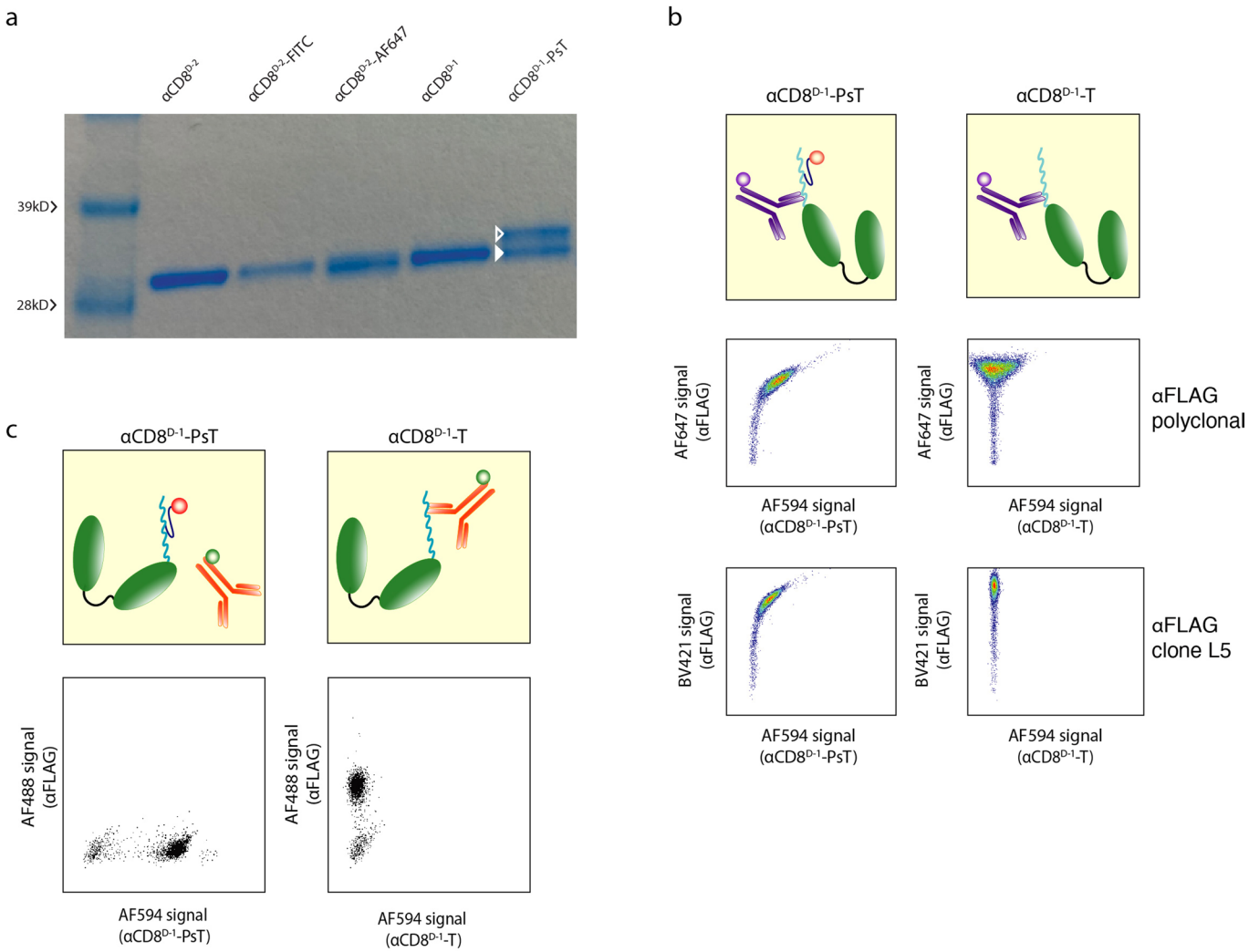

Extended Data Fig. 3 | αCD8-PsT nanobody generation and recognition by αFLAG antibodies. (**a**) Coomassie staining of sodium dodecyl sulfate polyacrylamide gel electrophoresis (SDS-PAGE) gel showing the indicated nanobodies before and after labeling with the PsT, FITC or AF647. Band marked with the open triangle represents the PsT-labeled αCD8^{D-1} and band marked with the closed triangle represents a hydrolysis product, that has previously been described in C-terminal protein labeling[39]. Data obtained from a single experiment. (**b**) Binding of αFLAG antibodies to the FLAG-tag with or without the NPBF cage (αCD8^{D-1}-PsT and αCD8^{D-1}-T respectively). Cells labeled with αCD8^{D-1}-PsT (left panel) or αCD8^{D-1}-T (right panel) were stained with polyclonal αFLAG antibodies or αFLAG clone L5. Data obtained from a single experiment. (**c**) Specific binding of αFLAG antibody clone D6W5B to the uncaged FLAG-tag. Cells stained with αCD8^{D-1} nanobody conjugated to either the FLAG-tag without cage (αCD8^{D-1}-T, upper panel) or the FLAG-tag containing the NPBF cage (αCD8^{D-1}-PsT, bottom panel) were stained with αFLAG antibody clone D6W5B. Note that appreciable AF488 signal is only observed when the uncaged FLAG-tag is used. Representative data from 3 independent experiments are depicted.

a

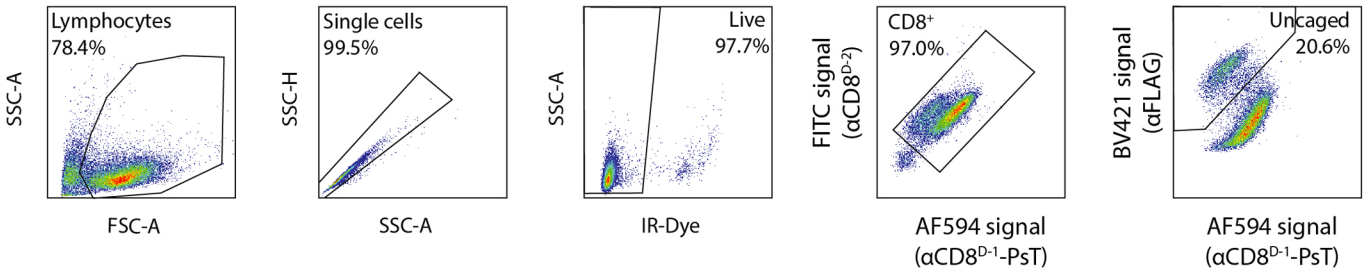

Extended Data Fig. 4 | Flow cytometry gating strategy to distinguish uncaged and caged CD8⁺ T cells. Data depict gating strategy used for flow cytometry analysis as well as for index sorting of uncaged CD8⁺ T cells. Viable single CD8⁺ T cells are selected based on double staining with αCD8^{D-1}-PsT and αCD8^{D-2}-FITC (serving as a stable signal to identify cells after loss of the AF594-positive cage). Uncaged cells are distinguished from caged cells based on their elevated αFLAG signal and reduced αCD8^{D-1}-PsT signal (AF594^{low} αFLAG^{high}).

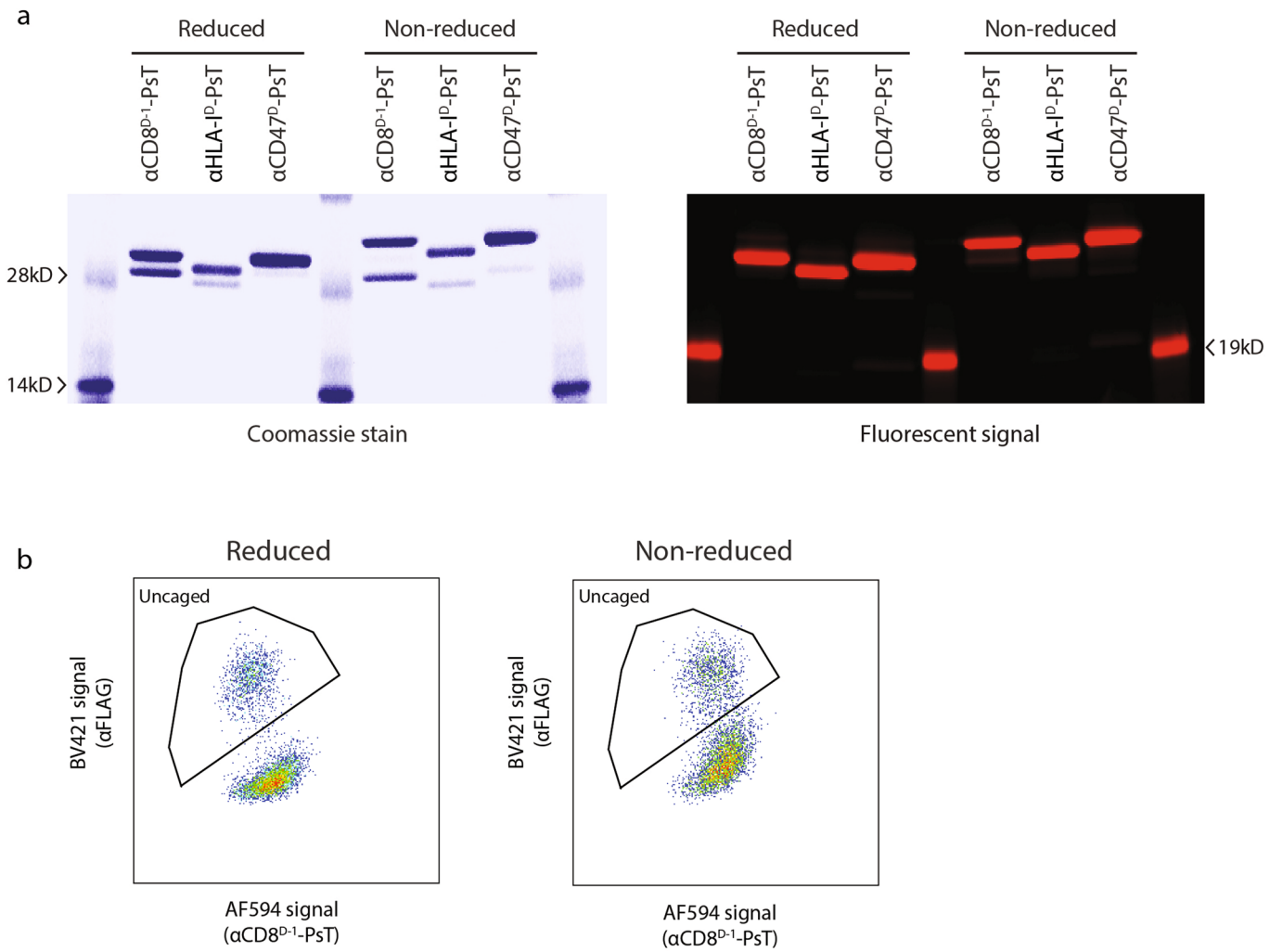

Extended Data Fig. 5 | Characterization of nanobodies labeled with monomeric or dimeric PsT. (**a**) SDS-PAGE analysis of nanobody-PsT generated under non-reducing or reducing conditions. Left panel: Coomassie stained SDS-PAGE gel showing the reduced (left) or non-reduced (right) versions of PsT-labeled αCD8^{D-1}, αCD47^{D} and αHLA-I^{D} nanobodies. Right panel: AF594 fluorescence signal of the same gel. Note the increased size of PsT-nanobodies when coupled under non-reducing conditions as compared to PsT-nanobodies generated under reducing condition, indicating the presence of PsT dimers under non-reducing conditions (see also LC-MS and NMR spectra in Supplementary Information). Lower band in both conditions represents the non-fluorescent hydrolysis product that is formed during sortase reactions[39]. Data obtained from a single experiment. (**b**) Flow cytometric analysis of the uncaging of CD8^{+} T cells labeled with αCD8^{D-1}-PsT nanobodies generated under reducing or non-reducing conditions (n = 2 technical replicates). Data were obtained from a single experiment.

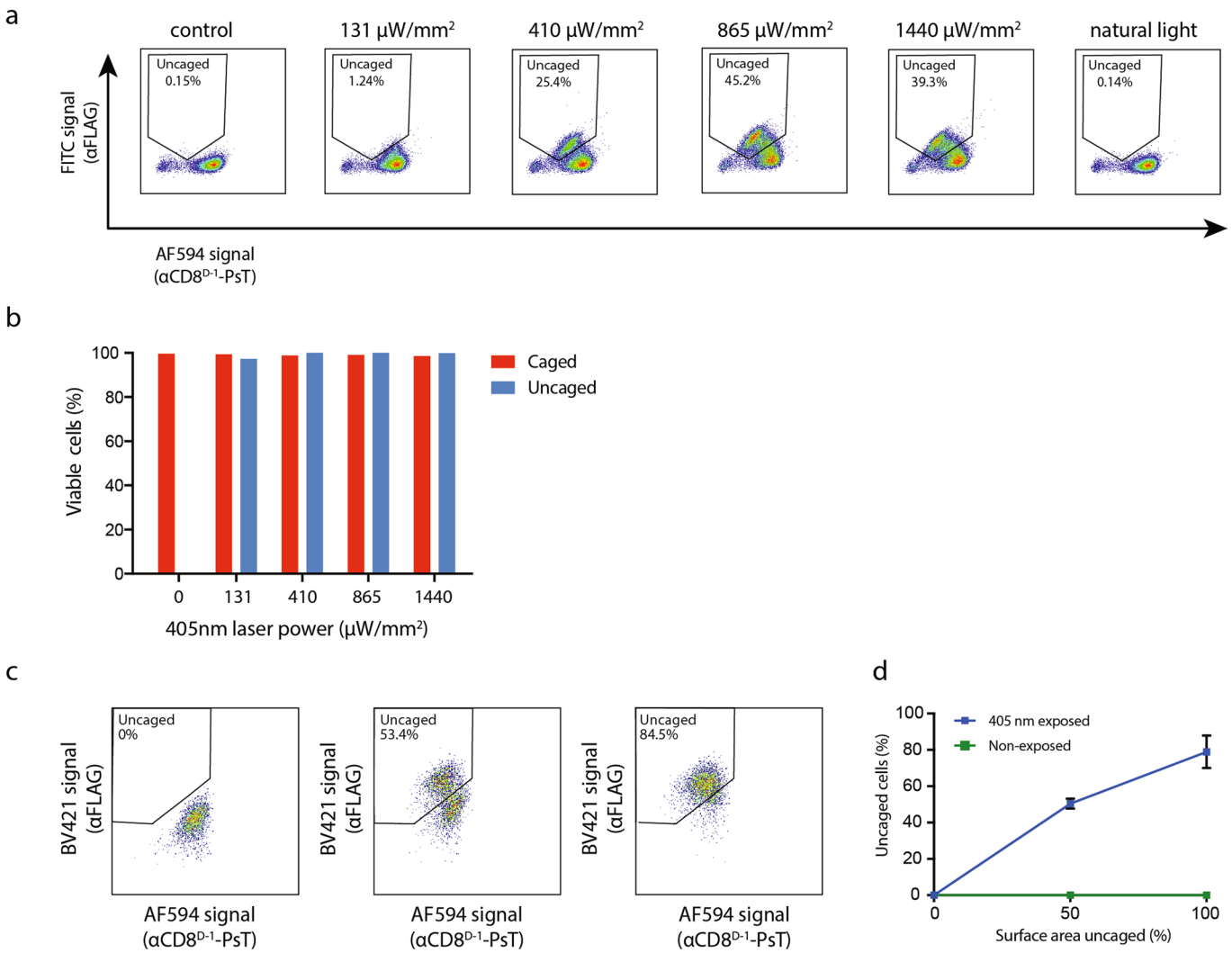

Extended Data Fig. 6 | Quantification of uncaging efficiency. (**a**) Flow cytometric analysis of αCD8^{D-1}-PsT-labeled CD8$^+$ T cells upon exposure to the indicated laser intensities or 1 hour to natural light. (**b**) Viability of uncaged (AF594^{low} αFLAG^{high}) or caged (AF594^{high} αFLAG^{low}) CD8$^+$ T cells from samples exposed to the indicated laser intensities, as measured by flow cytometric analysis following IR-dye live-dead staining. Data shown are obtained from a single experiment. (**c**) Correlation between uncaged surface area and the observed fraction uncaged αCD8^{D-1}-PsT labeled CD8$^+$ T cells in peripheral blood mononuclear cells (PBMCs). 0%, 50%, or 100% of the surface area of wells containing αCD8^{D-1}-PsT labeled cells was uncaged, and samples were analyzed by flow cytometry. (**d**) Quantification of the correlation between uncaged surface area and fraction uncaged CD8$^+$ T cells as measured with flow cytometry, as shown in Extended data Fig. 6c. After uncaging of the indicated surface areas, cells were mixed at a 1:1 ratio with PBMCs from non-exposed samples. Cells from exposed and non-exposed samples were distinguished by labeling samples with different αCD3 antibodies before mixing. Blue line represents the fraction of uncaged (AF594^{low} αFLAG^{high}) cells after local exposure with 405-nm light. Green line represents the fraction of AF594^{low} αFLAG^{high} cells within the second sample that was not exposed to 405-nm (that is not uncaged). Note that αCD8^{D-1}-PsT binding is stable throughout the experimental pipeline, as demonstrated by the absence of AF594^{low} αFLAG^{high} cells in the non-exposed sample. Line graphs show mean of technical triplicates from one experiment. Data are presented as mean values ± s.d.

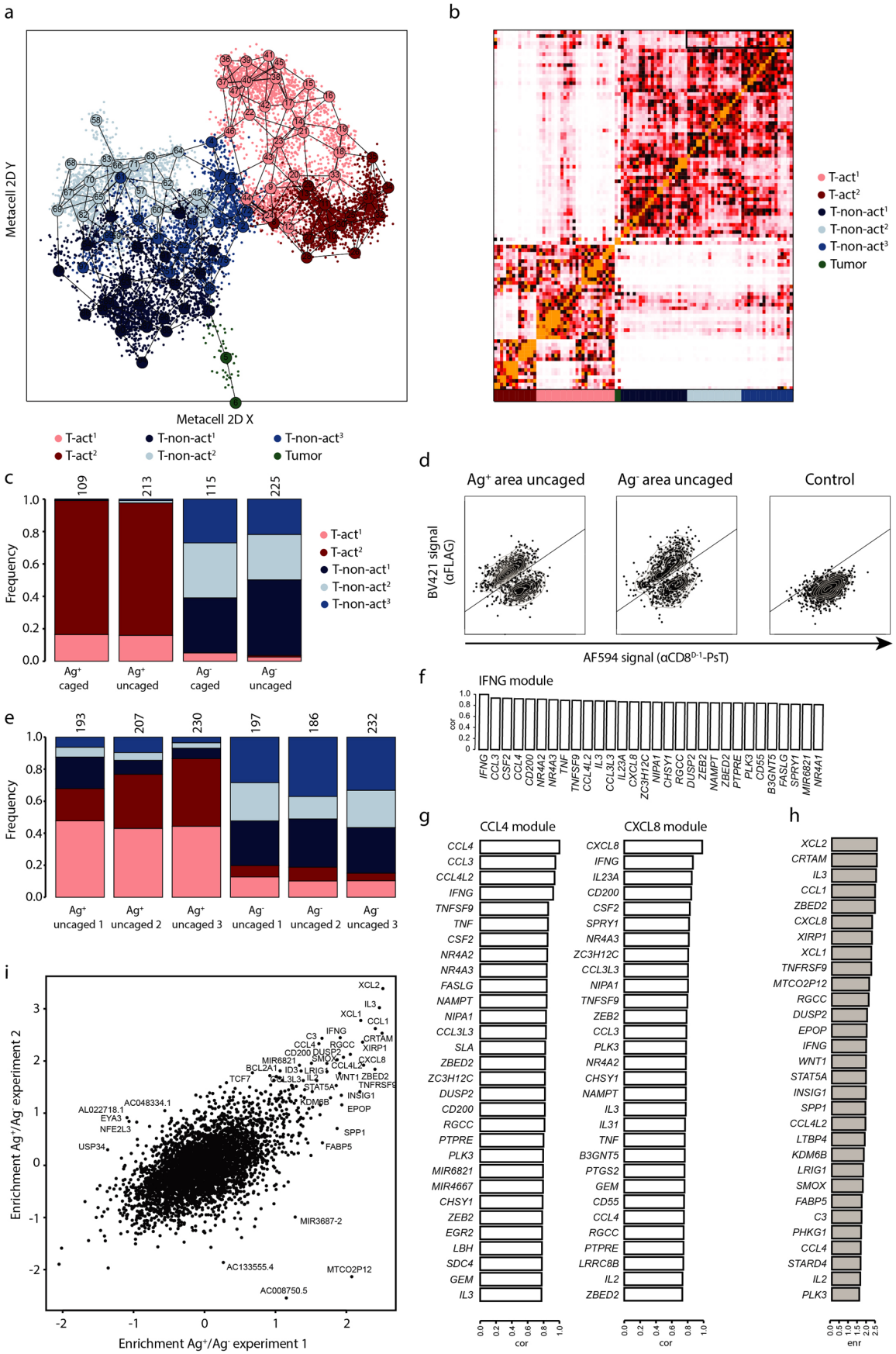

Extended Data Fig. 7 | See next page for caption.

Extended Data Fig. 7 | Single cell mRNA sequencing of locally activated CD8$^+$ T cells. (**a**) 2D projection of the 9,237 cells as shown in Fig. 4a divided into 99 metacells. Single cells are depicted as dots. Metacells are uniquely numbered and depicted as circles. Lines indicate relatedness between metacells. (**b**) Confusion matrix of all metacells. Clusters indicate groups of related metacells and are defined as main cell groups as shown by the color code below the confusion matrix that corresponds to the color code used in Fig. 4a and Extended data Fig. 7a. (**c**) Quantification of T cell states of uncaged (AF594^{low} αFLAG^{high}) CD8$^+$ T cell populations from control samples that only contained either Ag$^+$ or Ag$^-$ tumor cells, and in which an area was uncaged that is comparable to the areas uncaged in the tumor island conditions. Tumor cells are excluded from the analysis. Data are representative of 2 independent experiments. (**d**) αFLAG and αCD8^{D-1}-PsT signals, as acquired during index sorting. αFLAG and αCD8^{D-1}-PsT signals are depicted for those cells in the gene expression dataset that are derived from tumor island cultures in which either CD8$^+$ T cells in an Ag$^+$ area (left panel) or in an Ag$^-$ area (middle panel) were uncaged, or from the control condition (right panel) in which no cells were uncaged. Line depicts the cut-off between caged and uncaged CD8$^+$ T cells. (**e**) Quantification of T cell states for all technical replicates of uncaged (AF594^{low} αFLAG^{high}) CD8$^+$ T cells from antigen positive (Ag$^+$, 193–230 cells) and antigen negative (Ag$^-$, 186–232 cells) tumor cell areas. The three replicates jointly underlie the data in Fig. 4c. Tumor cells are excluded from the analysis. Representative data of 2 independent experiments. (**f**) Bar plots depicting the top 30 genes of which expression correlates most strongly with IFNG expression, together defining the *IFNG* module. (**g**) Bar plots depicting the top 30 genes of which expression correlates most strongly with the two alternative anchor genes *CCL4* (left) and *CXCL8* (right). (**h**) Gene expression enrichment in uncaged (AF594^{low} αFLAG^{high}) CD8$^+$ T cells from Ag$^+$ versus Ag$^-$ areas. Bar plot depicts the top 30 genes showing increased expression in uncaged CD8$^+$ T cells from an Ag$^+$ area as compared to uncaged CD8$^+$ T cells from an Ag$^-$ area. Gene enrichments are based on data from a single experiment. (**i**) Correlation of variable genes between uncaged CD8$^+$ T cells from Ag$^+$ versus Ag$^-$ areas in independent experiments. Scatterplot shows the gene enrichment scores in AF594^{low} αFLAG^{high} CD8$^+$ T cells from samples in which Ag$^+$ versus Ag$^-$ areas were uncaged for 2 independent experiments.

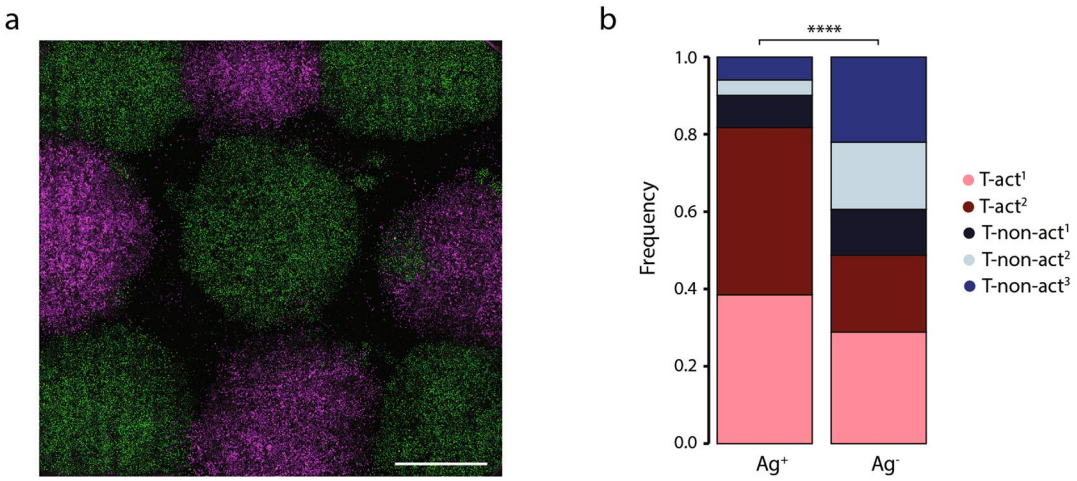

Extended Data Fig. 8 | Cell states from CD8⁺ T cells residing in intermingled tumor areas. (**a**) Confocal image of coculture of Ag-specific CD8⁺ T cells with tumor cell islands in which Ag⁺ tumor cell areas (green) and Ag⁻ tumor cell areas (magenta) are intermingled. Scale bar represents 2 mm. Representative of 2 independent experiments. (**b**) Quantification of T cell states in uncaged αCD8^{D-1}-PsT labeled CD8⁺ T cells from Ag⁺ and Ag⁻ areas in a mixed tumor culture as shown in Extended data Fig. 8a. Bar plots show the quantification of T cell states as defined in Fig. 4a of uncaged CD8⁺ T cell populations from samples in which either Ag⁺ or Ag⁻ areas were uncaged (252 and 236 cells, respectively). Tumor cells are excluded from the analysis. Two-tailed Chi-square test was performed (**** indicates $p < 1*10^{-15}$). Data shown were obtained in a single experiment.

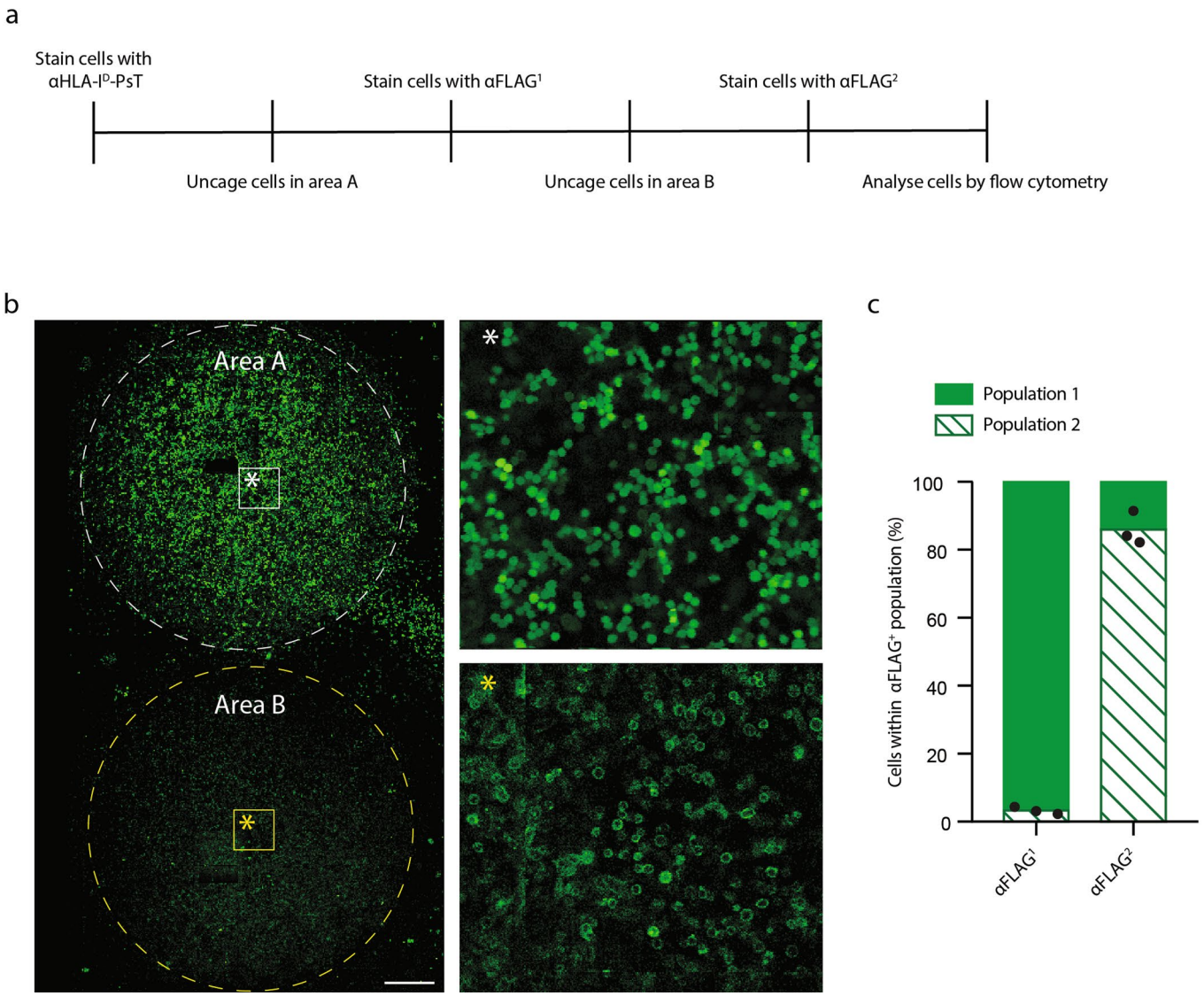

Extended data Fig. 9 | Multiplexed uncaging of cells in different areas. (**a**) Schematic representation of multiplexed analysis of cells in adjacent areas. (**b**) Representative confocal image of OVCAR5 tumor cell culture consisting of adjacent islands of GFP^+ cells (population 1) and GFP^- cells stained for expression of a cell membrane marker (population 2). Scale bar represents 250μm. Enlarged areas are indicated by the boxes. Tumor cells in a first island (area A, marked with the dashed white line), containing cells from population 1, were uncaged in a first uncaging round and *in situ* stained with a first fluorescently labeled αFLAG antibody ($\alpha FLAG^1$). Subsequently, tumor cells in a second island in the same culture (area B, marked by the dashed yellow line), containing cells from population 2, were uncaged in a second round of uncaging. After staining with a second fluorescent αFLAG antibody ($\alpha FLAG^2$), flow cytometric analysis was performed. Images are representative of 2 independent experiments. (**c**) Bar plot shows the fraction of population 1 (GFP^+) and population 2 (membrane-stained) cells within the $AF594^{low}$ and $\alpha FLAG^{1-high}$ (that is uncaged in round 1) population, or within the $AF594^{low}$ and $\alpha FLAG^{2-high}$ (that is uncaged in round 2) population (n = 3 technical replicates). Data are representative of 2 independent experiments.

nature research

Corresponding author(s): Ton N. Schumacher
Sander I. van Kasteren

Last updated by author(s): Jun 7, 2021

Reporting Summary

Nature Research wishes to improve the reproducibility of the work that we publish. This form provides structure for consistency and transparency in reporting. For further information on Nature Research policies, see our Editorial Policies and the Editorial Policy Checklist.

Statistics

For all statistical analyses, confirm that the following items are present in the figure legend, table legend, main text, or Methods section.

n/a	Confirmed	
☐	☒	The exact sample size (*n*) for each experimental group/condition, given as a discrete number and unit of measurement
☐	☒	A statement on whether measurements were taken from distinct samples or whether the same sample was measured repeatedly
☐	☒	The statistical test(s) used AND whether they are one- or two-sided *Only common tests should be described solely by name; describe more complex techniques in the Methods section.*
☒	☐	A description of all covariates tested
☒	☐	A description of any assumptions or corrections, such as tests of normality and adjustment for multiple comparisons
☐	☒	A full description of the statistical parameters including central tendency (e.g. means) or other basic estimates (e.g. regression coefficient) AND variation (e.g. standard deviation) or associated estimates of uncertainty (e.g. confidence intervals)
☐	☒	For null hypothesis testing, the test statistic (e.g. *F*, *t*, *r*) with confidence intervals, effect sizes, degrees of freedom and *P* value noted *Give P values as exact values whenever suitable.*
☒	☐	For Bayesian analysis, information on the choice of priors and Markov chain Monte Carlo settings
☒	☐	For hierarchical and complex designs, identification of the appropriate level for tests and full reporting of outcomes
☒	☐	Estimates of effect sizes (e.g. Cohen's *d*, Pearson's *r*), indicating how they were calculated

Our web collection on statistics for biologists contains articles on many of the points above.

Software and code

Policy information about availability of computer code

Data collection	BD FACSDiva 7, LASX 3.5.5
Data analysis	FlowJo 10.6.2, Prism version 8.0.0, R 3.6.2, RStudio 1.2.1335, MetaCell R package 3.41. The code reproducing the analyses in this study is available as supplementary file with the GEO accession GSE175813.

For manuscripts utilizing custom algorithms or software that are central to the research but not yet described in published literature, software must be made available to editors and reviewers. We strongly encourage code deposition in a community repository (e.g. GitHub). See the Nature Research guidelines for submitting code & software for further information.

Data

Policy information about availability of data

All manuscripts must include a data availability statement. This statement should provide the following information, where applicable:

- Accession codes, unique identifiers, or web links for publicly available datasets
- A list of figures that have associated raw data
- A description of any restrictions on data availability

The processed single cell RNA sequencing data are deposited in the NCBI GEO under accession number GSE175813.

Field-specific reporting

Please select the one below that is the best fit for your research. If you are not sure, read the appropriate sections before making your selection.

☒ Life sciences ☐ Behavioural & social sciences ☐ Ecological, evolutionary & environmental sciences

For a reference copy of the document with all sections, see nature.com/documents/nr-reporting-summary-flat.pdf

Life sciences study design

All studies must disclose on these points even when the disclosure is negative.

Sample size	No expected effect size was pre-specified. Generally accepted sample sizes were used, with a significant difference between conditions indicating that the sample size is sufficient. For key experiments, at least 2 independent experiments containing technical replicates were performed.
Data exclusions	Single cell RNA sequencing data were filtered as described in the methods. "Cells with less than 500 UMIs were filtered out, as well as cells with a fraction of mitochondrial gene expression that exceeded 0.6." These cutoffs were previously established in Li et al (Cell 2018). No further data were excluded from the analyses.
Replication	Every figure states how many times each experiment has been repeated. To ensure experiments could be reliably reproduced, fully independent experiments were performed for most experiments, as defined by commonly accepted standards.
Randomization	Tumor fragments were randomly distributed over the different uncaging conditions. For experiments with cultured cells, cells derived from the same pool were equally divided over the conditions used in every experiment.
Blinding	Flow cytometry analyses were not performed blinded since signals from experimental conditions were compared directly to control samples within the same experiment. For single cell RNA analyses, cells from the different conditions were clustered together independent of their uncaging status. After assigning the clusters, cluster abundance was determined for each uncaging condition.

Reporting for specific materials, systems and methods

We require information from authors about some types of materials, experimental systems and methods used in many studies. Here, indicate whether each material, system or method listed is relevant to your study. If you are not sure if a list item applies to your research, read the appropriate section before selecting a response.

Materials & experimental systems

n/a	Involved in the study
☐	☒ Antibodies
☐	☒ Eukaryotic cell lines
☒	☐ Palaeontology and archaeology
☒	☐ Animals and other organisms
☒	☐ Human research participants
☒	☐ Clinical data
☒	☐ Dual use research of concern

Methods

n/a	Involved in the study
☒	☐ ChIP-seq
☐	☒ Flow cytometry
☒	☐ MRI-based neuroimaging

Antibodies

Antibodies used

Antibodies Clone Fluorophore cat nr supplier LOT Dilution
aFLAG D6W5B AF647 15009 Cell signaling technology 3 1:50
aFLAG D6W5B cold 147935 Cell signaling technology 5 1:800
aFLAG poly AF647 3916 Cell signaling technology 12 1:200
aFLAG L5 BV421 637321 biolegend B274095 1:50
CD3 UCTH1 BV711 563725 BD Biosciences 8164658 1:100
CD3 SK7 FITC BD Biosciences 345764 0009584 1:30
CD3 SK7 APC BD Biosciences 345767 9018851 1:30
Goat Anti-Rabbit IgG Poly BV421 565014 BD Biosciences 9262477 1:200
CD69 FN50 PeCy7 310911 Biolegend B285204 1:100
maleimide AF647 NA AF647 A20347 Thermo Fisher Scientific 1749854 1mg/labeling reaction
maleimide FITC NA FITC F150 Thermo Fisher Scientific 1mg/labeling reaction
HLA A2 BB7.2 FITC 551285 BD Biosciences 5107562 1:50
IFNgR GIR-208 PE 12-1199-41 Ebioscience 4277721 1:50
CD44 IM7 AF647 103017 Biolegend 1:50

Validation	All antibodies were validated for their application by the manufacturer (see above in "Antibodies used" for details). aFLAG cold and Goat-anti-rabbit antibodies were titrated before use in the experiments. Labeled nanobody batches were titrated before use. Specificity of staining was assessed for all antibodies used in this study by comparing the fluorescent signal to control conditions.

Eukaryotic cell lines

Policy information about cell lines

Cell line source(s)	Sources of all the cell lines are indicated in the methods section. OVCAR5 cells were kindly provided by Dr. F. Scheeren. BA/F3 cells were kindly provided by J. Leusen.
Authentication	OVCAR5 cells have been validated by STR analysis.
Mycoplasma contamination	Cell lines have been tested negative for Mycoplasma contamination
Commonly misidentified lines (See ICLAC register)	No commonly misidentified lines were used in this study.

Flow Cytometry

Plots

Confirm that:

☒ The axis labels state the marker and fluorochrome used (e.g. CD4-FITC).

☒ The axis scales are clearly visible. Include numbers along axes only for bottom left plot of group (a 'group' is an analysis of identical markers).

☒ All plots are contour plots with outliers or pseudocolor plots.

☒ A numerical value for number of cells or percentage (with statistics) is provided.

Methodology

Sample preparation	All cells were stained in PBS supplemented with 0.5% BSA (Sigma) and EDTA (2 mM, Life Technologies) for 30 minutes at 4 oC.
Instrument	BD LSRFortessa™ Flow Cytometer, BD FACSAria™ Fusion Cell Sorter
Software	FACSDiva 7, FlowJo 10.6.2
Cell population abundance	The sorted T cells were > 90% pure as shown by the cell state analysis done based on the downstream single cell RNA sequencing analysis.
Gating strategy	Lymphocyte gating (FCS-A/SSC-A) - single cells (SSC-H/SSC-A) - live cells (IRdye neg) - Pst labeled CD8 T cells (aCD8 FITC/ aCD8 AF594) - uncaging (aFLAG BV421 high / aCD8 AF594 low)

☒ Tick this box to confirm that a figure exemplifying the gating strategy is provided in the Supplementary Information.